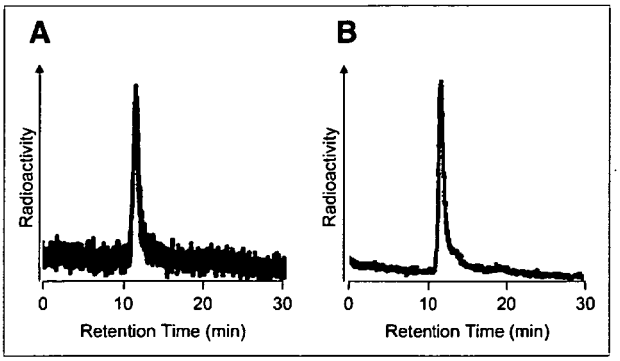

FIGURE 4. RP-HPLC chromatograms of ^{99m}Tc-HYNIC-HBP prepared by coupling of [^{99m}Tc](HYNIC-TFP)(tricine)(3-acetylpyridine) with bisphosphonate derivative (A) and labeling of HYNIC-HBP with $^{99m}TcO_4^-$, tricine, and 3-acetylpyridine (B). Conditions: flow rate of 1 mL/min with 10% ethanol in 200 mmol/L phosphate buffer (pH 6.0) containing 10 mmol/L tetrabutylammoniumhydroxide.

These results indicate that ^{99m}Tc-HYNIC-HBP holds great potential for bone scintigraphy.

ACKNOWLEDGMENTS

This work was supported in part by a Grant-in-Aid for Scientific Research from the Ministry of Education, Culture, Sports, Science and Technology of Japan and a research grant from the Sagawa Foundation for Promotion of Cancer Research.

REFERENCES

1. Subramanian G, McAfee JG, Blair RJ, Kallfelz FA, Thomas FD. Technetium-99m-methylene diphosphonate: a superior agent for skeletal imaging—comparison with other technetium complexes. *J Nucl Med.* 1975;16:744–755.
2. Domstad PA, Coupal JJ, Kim EE, Blake JS, DeLand FH. ^{99m}Tc-Hydroxymethane diphosphonate: a new bone imaging agent with a low tin content. *Radiology.* 1980;136:209–211.
3. Love C, Din AS, Tomas MB, Kalapparambath TP, Palestro CJ. Radionuclide bone imaging: an illustrative review. *Radiographics.* 2003;23:341–358.
4. Mari C, Catafau A, Carrio I. Bone scintigraphy and metabolic disorders. *Q J Nucl Med.* 1999;43:259–267.
5. Meyer JL, Nancollas GH. The influence of multidentate organic phosphonates on the crystal growth of hydroxyapatite. *Calcif Tissue Res.* 1973;13:295–303.
6. Libson K, Deutsch E, Barnett BL. Structural characterization of a technetium-99-diphosphonate complex: implications for the chemistry of technetium-99m skeletal imaging agents. *J Am Chem Soc.* 1980;102:2476–2478.
7. Hnatowich DJ, Qu T, Chang F, Ley AC, Ladner RC, Rusckowski M. Labeling peptides with technetium-99m using a bifunctional chelator of a N-hydroxysuccinimide ester of mercaptoacetyltriglycine. *J Nucl Med.* 1998;39:56–64.
8. Liu S, Edwards DS, Barrett JA. ^{99m}Tc labeling of highly potent small peptides. *Bioconjug Chem.* 1997;8:621–636.
9. Abrams MJ, Juweid M, tenKate CI, et al. Technetium-99m-human polyclonal IgG radiolabeled via the hydrazino nicotinamide derivative for imaging focal sites of infection in rats. *J Nucl Med.* 1990;31:2022–2028.
10. Ohtsuki K, Akashi K, Aoka Y, et al. Technetium-99m HYNIC-annexin V: a potential radiopharmaceutical for the in-vivo detection of apoptosis. *Eur J Nucl Med.* 1999;26:1251–1258.
11. Steffens MG, Oosterwijk E, Kranenborg MH, et al. In vivo and in vitro characterizations of three ^{99m}Tc-labeled monoclonal antibody G250 preparations. *J Nucl Med.* 1999;40:829–836.
12. Ogawa K, Mukai T, Arano Y, et al. Development of a rhenium-186-labeled MAG3-conjugated bisphosphonate for the palliation of metastatic bone pain based on the concept of bifunctional radiopharmaceuticals. *Bioconjug Chem.* 2005;16:751–757.
13. Ono M, Arano Y, Mukai T, et al. ^{99m}Tc-HYNIC-derivatized ternary ligand complexes for ^{99m}Tc-labeled polypeptides with low in vivo protein binding. *Nucl Med Biol.* 2001;28:215–224.
14. Fujisawa R, Kuboki Y. Preferential adsorption of dentin and bone acidic proteins on the (100) face of hydroxyapatite crystals. *Biochim Biophys Acta.* 1991;1075:56–60.
15. Kasugai S, Fujisawa R, Waki Y, Miyamoto K, Ohya K. Selective drug delivery system to bone: small peptide $(Asp)_6$ conjugation. *J Bone Miner Res.* 2000;15:936–943.
16. Ogawa K, Mukai T, Arano Y, et al. Rhenium-186-monoaminemonoamidedithiol-conjugated bisphosphonate derivatives for bone pain palliation. *Nucl Med Biol.* 2006;33:513–520.
17. Fritzberg AR, Kasina S, Eshima D, Johnson DL. Synthesis and biological evaluation of technetium-99m MAG3 as a hippuran replacement. *J Nucl Med.* 1986;27:111–116.
18. Verbruggen AM, Nosco DL, Van Nerom CG, Bormans GM, Adriaens PJ, De Roo MJ. Technetium-99m-L,L-ethylenedicysteine: a renal imaging agent. I. Labeling and evaluation in animals. *J Nucl Med.* 1992;33:551–557.
19. Taylor A Jr, Eshima D, Christian PE, Wooten WW, Hansen L, McElvany K. Technetium-99m MAG3 kit formulation: preliminary results in normal volunteers and patients with renal failure. *J Nucl Med.* 1988;29:616–622.
20. Verbeke K, Hjelstuen O, Debrock E, Cleynhens B, De Roo M, Verbruggen A. Comparative evaluation of ^{99}Tc^m-Hynic-HSA and ^{99}Tc^m-MAG3-HSA as possible blood pool agents. *Nucl Med Commun.* 1995;16:942–957.
21. Van der Laken CJ, Boerman OC, Oyen WJG, et al. Technetium-99m-labeled chemotactic peptides in acute infection and sterile inflammation. *J Nucl Med.* 1997;38:1310–1315.
22. Liu S, Edwards DS, Looby RJ, et al. Labeling a hydrazino nicotinamide-modified cyclic IIb/IIIa receptor antagonist with ^{99m}Tc using aminocarboxylates as coligands. *Bioconjug Chem.* 1996;7:63–71.
23. Ono M, Arano Y, Uehara T, et al. Intracellular metabolic fate of radioactivity after injection of technetium-99m-labeled hydrazino nicotinamide derivatized proteins. *Bioconjug Chem.* 1999;10:386–394.
24. Ono M, Arano Y, Mukai T, et al. Plasma protein binding of ^{99m}Tc-labeled hydrazino nicotinamide derivatized polypeptides and peptides. *Nucl Med Biol.* 2001;28:155–164.
25. Liu S, Edwards DS, Harris AR. A novel ternary ligand system for ^{99m}Tc-labeling of hydrazino nicotinamide-modified biologically active molecules using imine-N-containing heterocycles as coligands. *Bioconjug Chem.* 1998;9:583–595.
26. Vallner JJ. Binding of drugs by albumin and plasma protein. *J Pharm Sci.* 1977;66:447–465.
27. Daneshmend TK, Warnock DW. Clinical pharmacokinetics of systemic antifungal drugs. *Clin Pharmacokinet.* 1983;8:17–42.
28. Ogiso T, Iwaki M, Konishi Y. Effect of furosemide on plasma clearance, anticoagulant effect and protein binding of warfarin in rats. *J Pharmacobiodyn.* 1982;5:829–840.
29. van Langevelde A, Driessen OMJ, Pauwels EKJ, Thesingh CW. Aspects of ^{99m}technetium binding from an ethane-1-hydroxy-1,1-diphosphonate ^{99m}Tc complex to bone. *Eur J Nucl Med.* 1977;2:47–51.
30. Schwartz Z, Shani J, Soskolne WA, Touma H, Amir D, Sela J. Uptake and biodistribution of technetium-99m-MD^{32}P during rat tibial bone repair. *J Nucl Med.* 1993;34:104–108.

Available online at www.sciencedirect.com
SCIENCE DIRECT
Nuclear Medicine and Biology 33 (2006) 513–520
NUCLEAR MEDICINE — AND — BIOLOGY
www.elsevier.com/locate/nucmedbio

Rhemium-186-monoaminemonoamidedithiol-conjugated bisphosphonate derivatives for bone pain palliation

Kazuma Ogawa[a,b], Takahiro Mukai[a,c], Yasushi Arano[d], Akira Otaka[a], Masashi Ueda[a], Tomoya Uehara[d], Yasuhiro Magata[e], Kazuyuki Hashimoto[f], Hideo Saji[a,*]

[a]*Graduate School of Pharmaceutical Sciences, Kyoto University, Yoshida Shimoadachi-cho, Sakyo-ku, Kyoto 606-8501, Japan*
[b]*Advanced Science Research Center, Kanazawa University, Kanazawa 920-8640, Japan*
[c]*Graduate School of Pharmaceutical Sciences, Kyushu University, Higashi-ku, Fukuoka 812-8582, Japan*
[d]*Graduate School of Pharmaceutical Sciences, Chiba University, Chuo-ku, Chiba 260-8675, Japan*
[e]*Photon Medical Research Center, Hamamatsu University School of Medicine, Hamamatsu 431-3192, Japan*
[f]*Japan Atomic Energy Research Institute, Tokai-mura, Ibaraki 319-1195, Japan*

Received 14 October 2005; received in revised form 17 March 2006; accepted 17 March 2006

Abstract

To develop a radiopharmaceutical for the palliation of painful bone metastases based on the concept of bifunctional radiopharmaceuticals, we synthesized a bisphosphonate derivative labeled with rhenium-186 (^{186}Re) that contains a hydroxyl group at the central carbon of its bisphosphonate structure, we attached a stable ^{186}Re-MAMA chelate to the amino group of a 4-amino-butylidene-bisphosphonate derivative [*N*-[2-[[4-[(4-hydroxy-4,4-diphosphonobutyl)amino]-4-oxobutyl]-2-thioethylamino]acetyl]-2-aminoethanethiolate] oxorhenium (V) (^{186}Re-MAMA-HBP) and we investigated the effect of a hydroxyl group at the central carbon of its bisphosphonate structure on affinity for hydroxyapatite and on biodistribution by conducting a comparative study with [*N*-[2-[[3-(3,3-diphosphonopropylcarbamoyl)propyl]-2-thioethylamino]acetyl]-2-aminoethanethiolate] oxorhenium (V) (^{186}Re-MAMA-BP). The precursor of ^{186}Re-MAMA-HBP, trityl (Tr)-MAMA-HBP, was obtained by coupling a Tr-MAMA derivative to 4-amino-1-hydroxybutylidene-1,1-bisphosphonate. ^{186}Re-MAMA-HBP was prepared by a reaction with $^{186}ReO_4^-$ and $SnCl_2$ in citrate buffer after the deprotection of the Tr groups of Tr-MAMA-HBP. After reversed-phase high-performance liquid chromatography, ^{186}Re-MAMA-HBP had a radiochemical purity of over 95%. Compared with ^{186}Re-MAMA-BP, ^{186}Re-MAMA-HBP showed a greater affinity for hydroxyapatite beads in vitro and accumulated a significantly higher level in the femur in vivo. Thus, the introduction of a hydroxyl group into ^{186}Re complex-conjugated bisphosphonates would be effective in enhancing accumulation in bones. These findings provide useful information on the design of bone-seeking therapeutic radiopharmaceuticals.

Keywords: Rhenium-186; Monoaminemonoamidedithiols; Bisphosphonate; Bone; Palliation

1. Introduction

Many cancers, especially breast and prostate carcinomas, have a strong propensity to metastasize to the bone [1]. Bone metastases are usually associated with severe pain, which has an important impact on quality of life [2]. Standard treatment options for bone metastases include external beam radiotherapy [3], while internal radiotherapy with radiopharmaceuticals would be preferable if the patient has a large number of metastatic lesions [4,5].

Rhenium-186 (^{186}Re) is a useful radionuclide for internal radiotherapy. Thus, rhenium-186-1-hydroxyethylidene-1, 1-diphosphonate (^{186}Re-HEDP) has been used for the palliation of metastatic bone pain [6-9]. However, ^{186}Re-HEDP showed delayed blood clearance and high gastric uptake of radioactivity upon injection [10]. These features were attributed to the generation of $^{186}ReO_4^-$ resulting from the instability of this ^{186}Re complex in vivo [11,12]. To improve the instability of ^{186}Re-HEDP based on the concept of bifunctional radiopharmaceuticals, we recently developed

* Corresponding author. Department of Patho-Functional Bioanalysis, Graduate School of Pharmaceutical Sciences, Kyoto University, Yoshida Shimoadachi-cho, Sakyo-ku, Kyoto 606-8501, Japan. Tel.: +81 75 753 4556; fax: +81 75 753 4568.
E-mail address: hsaji@pharm.kyoto-u.ac.jp (H. Saji).

0969-8051/$ – see front matter © 2006 Elsevier Inc. All rights reserved.
doi:10.1016/j.nucmedbio.2006.03.006

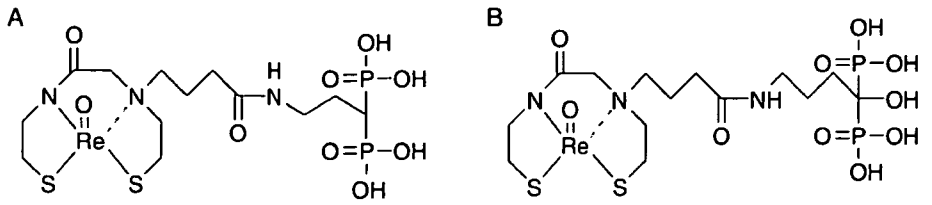

Fig. 1. Chemical structures of (A) Re-MAMA-BP and (B) Re-MAMA-HBP.

a new ^{186}Re-labeled bisphosphonate derivative through the conjugation of a stable ^{186}Re complex to a bisphosphonate analog [*N*-[2-[[3-(3,3-diphosphonopropylcarbamoyl)propyl]-2-thioethylamino]acetyl]-2-aminoethanethiolate] oxorhenium (V) (^{186}Re-MAMA-BP); Fig. 1A]. As expected, ^{186}Re-MAMA-BP was considerably more stable than ^{186}Re-HEDP in vitro [13].

Previous studies of bisphosphonates suggest that a hydroxyl group at a central carbon of the bisphosphonate structure affects the affinity for bone minerals [14,15]. Since extensive accumulation in bones is a definitive requirement for a therapeutic drug in the palliation of metastatic bone pain, we designed a ^{186}Re-MAMA-BP derivative with a hydroxyl group at a central carbon of the bisphosphonate structure, [*N*-[2-[[4-[(4-hydroxy-4,4-diphosphonobutyl)-amino]-4-oxobutyl]-2-thioethylamino]acetyl]-2-aminoethanethiolate]oxorhenium(V) **(6)** (^{186}Re-MAMA-HBP; Fig. 1B) in order to develop a ^{186}Re-labeled compound with greater accumulation in the bone. In this study, we synthesized ^{186}Re-MAMA-HBP and evaluated the effect of introducing a hydroxyl group at a central carbon of the bisphosphonate structure on the affinity for hydroxyapatite and on in vivo accumulation in the bone by studying and comparing it with ^{186}Re-HEDP and ^{186}Re-MAMA-BP.

2. Materials and methods

2.1. Materials

Ion spray mass spectrum was obtained with an API*III*E triple quadrupole mass spectrometer (Perkin-Elmer Science Instruments, Thornhill, Canada). Thin-layer chromatography (TLC) analyses were performed with silica plates (Silica Gel 60; Merck KGaA, Darmstadt, Germany), with acetone as developing solvent. ^{186}Re was supplied as $^{186}ReO_4^-$ by the Japan Atomic Energy Research Institute (Ibaraki, Japan) [16]. ^{186}Re-MAMA-BP and ^{186}Re-HEDP

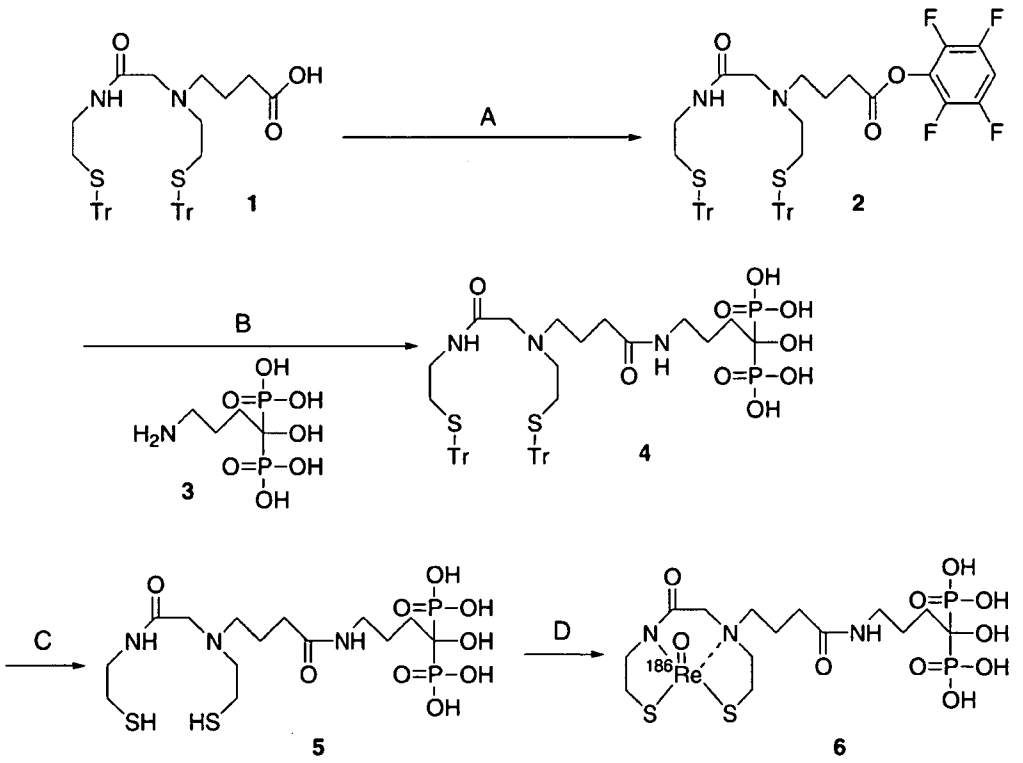

Scheme 1. Synthesis of ^{186}Re-MAMA-HBP. Reagents: (A) TFP and DCC; (B) Et_3N; (C) TFA and triethylsilane; (D) $^{186}ReO_4^-$ and $SnCl_2$/citrate.

were synthesized as described previously [13]. Other reagents were of reagent grade and were used as received.

2.2. Synthesis of ^{186}Re-MAMA-HBP

^{186}Re-MAMA-HBP was synthesized according to the procedure outlined in Scheme 1.

2.2.1. N^2-[4-[(4-hydroxy-4,4-diphosphonobutyl)amino]-4-oxobutyl]-N^1,N^2-bis[2-(tritylthio)ethyl]glycinamide [trityl (Tr)-MAMA-HBP] (4)

N-[2-(Tritylthio)ethylaminocarbonylmethyl]-*N*-[2-(tritylthio)ethyl]-4-aminobutyric acid **(1)** (172 mg, 0.225 mmol), synthesized as described previously [13], and tetrafluorophenol (TFP) (43.6 mg, 0.248 mmol) were dissolved in 3 ml of chloroform. Dicyclohexylcarbodiimide (DCC; 51.6 mg, 0.248 mmol) in 4 ml of chloroform was added dropwise to the reaction mixture at room temperature. After 1 h of stirring at room temperature, the solvent was removed in vacuo. The residue was then suspended in an adequate volume of ethyl acetate, DCC urea was removed by filtration and the filtrate was evaporated in vacuo to obtain crude [*N*-[2-(tritylthio)ethylaminocarbonylmethyl]-*N*-[2-(tritylthio)ethyl]-4-aminobutyric acid 2,3,5,6-tetrafluorophenyl ester (2). Compound **(2)** was used in the next reaction without further purification. 4-Amino-1-hydroxybutylidene-1,1-bisphosphonate **(3)** (57.0 mg, 0.229 mmol), synthesized according to the method of Kieczykowski [17], was suspended in 3 ml of distilled water, and triethylamine (140 mg, 1.39 mmol) was added to the suspension. After a few seconds of stirring at room temperature, the suspension became clear. Compound **(2)** was dissolved in 4 ml of acetonitrile and was then added to the reaction mixture. Triethylamine (23.3 mg, 231 μmol) was then added, and the reaction mixture was stirred for 3 h at room temperature. This mixture was purified by reversed-phase high-performance liquid chromatography (RP-HPLC), which was performed with a Cosmosil $5C_{18}$-AR-300 column (10× 150 mm; Nacalai Tesque, Kyoto, Japan) at a flow rate of 4.7 ml/min with a gradient mobile phase from 5% acetonitrile in water with 0.1% trifluoroacetic acid (TFA) to 100% acetonitrile with 0.1% TFA for 30 min. Chromatograms were obtained by monitoring ultraviolet adsorption at a wavelength of 254 nm. The fraction containing Tr-MAMA-HBP **(4)** was determined by mass spectrometry and then collected. The solvent was removed by lyophilization to provide Tr-MAMA-HBP **(4)** (66.0 mg, 29.5%) as white crystals [ion spray mass spectrum calculated for $C_{52}H_{59}N_3O_9P_2S_2$ $(M+H)^+$: *m/z* 996; found: 996].

2.2.2. ^{186}Re-MAMA-HBP (6)

The Tr groups of Tr-MAMA-HBP were deprotected just before radiolabeling. Tr-MAMA-HBP **(4)** (0.3 mg) was dissolved in 190 μL of TFA and 10 μL of triethylsilane and then gently shaken. After the removal of the solvent under a stream of N_2, 0.1 ml of 0.2 M acetate buffer (pH 3.0) was added to the residue. To this solution were added stannous chloride (0.3 mg) in 0.1 ml of 0.1 M citrate buffer (pH 5.0) and 0.1 ml of $^{186}ReO_4^-$ solution. The mixture was vigorously stirred and allowed to react at 90°C for 1 h. After cooling to room temperature, ^{186}Re-MAMA-HBP was purified by RP-HPLC (Cosmosil $5C_{18}$-AR-300 column, 4.6×150 mm) and eluted with a mixture of 0.2 M phosphate buffer (pH 6.0) and ethanol (85:15) containing 10 mM tetrabutylammonium hydroxide at a flow rate of 1 ml/min. Radiochemical purity was determined by RP-HPLC and TLC.

2.3. In vitro stability

To evaluate the stability of ^{186}Re-MAMA-HBP in vitro, ^{186}Re-MAMA-HBP was diluted with 0.1 M phosphate buffer (pH 7.0) saturated with 95% O_2/5% CO_2, and the solution was incubated at 37°C for 24 h. After 1, 3, 6 and 24 h of incubation, the samples were drawn, and radioactivity was analyzed by RP-HPLC and TLC.

2.4. Biodistribution experiments

Animal experiments were conducted in accordance with our institutional guidelines, and experimental procedures were approved by the Kyoto University Animal Care Committee. Biodistribution experiments were performed by the intravenous administration of ^{186}Re-labeled compounds to 6-week-old male ddY mice (27–30 g). Groups of five or six mice each were administered 100 μL of each ^{186}Re-labeled compound and sacrificed at 10 min, 1 h, 3 h, 6 h and 24 h postinjection. Tissues of interest were removed and weighed. The whole left femur was isolated as a representative bone sample. Radioactivity levels in these tissues were determined with an autowell gamma counter (ARC 2000; Aloka, Tokyo, Japan).

2.5. Hydroxyapatite binding assay

The binding assay was performed as described previously, with slight modifications [18,19]. In brief, hydroxyapatite beads (Bio-Gel; Bio-Rad, Hercules, CA) were suspended in Tris/HCl-buffered saline (50 mM, pH 7.4) at 1, 10 and 25 mg/ml. One hundred microliters of ^{186}Re-MAMA-HBP, ^{186}Re-MAMA-BP or ^{186}Re-HEDP was added to the suspension (100 μL), and the mixture was gently shaken for 1 h at room temperature. After centrifugation at 10,000×*g* for 5 min, the radioactivity of the supernatant was measured. Control experiments were performed with a similar procedure in the absence of hydroxyapatite beads. The binding ratios were determined as follows:

$$\text{Hydroxyapatite binding (\%)} = 1 - \frac{\text{radioactivity of the supernatant of each sample}}{\text{radioactivity of the supernatant in the respective control}} \times 100.$$

The effect of bisphosphonate on the binding of ^{186}Re-MAMA-HBP to hydroxyapatite beads was also examined.

Table 1
Stability of ^{186}Re-MAMA-HBP in buffered solution

Incubation period (h)	Radiochemical purity (%)	S.D.
0	97.95	0.33
1	98.50	0.65
3	97.55	1.17
6	94.91	0.27
24	75.55	1.57

Each value represents the mean (S.D.) for three experiments.

One hundred microliters of ^{186}Re-MAMA-HBP, which additionally contained a different amount of HEDP, was incubated with 100 μL of the suspension containing 1 mg of hydroxyapatite beads. After centrifugation, the radioactivity of the supernatant was measured.

2.6. Determination of the partition coefficient

The partition coefficients of ^{186}Re-labeled compounds were measured as follows: a 10-μL aliquot of ^{186}Re-labeled compound was mixed with 3 g each of 1-octanol and phosphate buffer (0.1 M, pH 7.4) in a test tube. The mixture was vortexed (3×1 min) then stood for 20 min. After the procedure had been repeated thrice, the mixture was centrifuged at 1000×*g* for 5 min. Two 1-ml aliquots of each phase were removed, and their radioactivity was measured with a well counter. The partition coefficient was determined by calculating the ratio of 1-octanol to the buffer and was expressed as a common logarithm (log PC).

2.7. Radiation dose estimates

Residence times were calculated by monoexponential extrapolation of biodistribution data. According to residence times, radiation doses were calculated for adult patients using the MIRDOSE 3.1 program.

2.8. Statistical analysis

Throughout this paper, data are expressed as mean±S.D. In biodistribution experiments, data were compared for each time point using the Tukey–Kramer test. In hydroxyapatite binding experiments, the binding rates of ^{186}Re-MAMA-BP and ^{186}Re-MAMA-HBP for each concentration of hydroxyapatite were compared using unpaired Student's *t* test. $P = .05$ was defined as the limit of significance.

3. Results

3.1. Preparation of ^{186}Re-MAMA-HBP

For the synthesis of the precursor of ^{186}Re-MAMA-BP, Tr-MAMA-BP, a bisphosphoric tetraethyl ester derivative was conjugated with compound **(1)** (Tr-MAMA derivative) in the presence of DCC. After the hydrolysis of tetraethyl esters, Tr-MAMA-BP was obtained in good yield [13]. However, for the synthesis of the ^{186}Re-MAMA-HBP precursor, Tr-MAMA-HBP, bisphosphoric tetraalkyl esters with a hydroxyl group at the central carbon could not be synthesized. Thus, a bisphosphonate derivative **(3)** that has no protecting

Table 2
Biodistribution of radioactivity after intravenous administration of ^{186}Re-MAMA-HBP, ^{186}Re-MAMA-BP and ^{186}Re-HEDP in mice

Tissue	Time after administration				
	10 min	1 h	3 h	6 h	24 h
^{186}Re-MAMA-HBP					
Blood[a]	3.15[b] (0.46)	0.27[b,c] (0.04)	0.12[b,c] (0.03)	0.07[c] (0.01)	0.02[c] (0.01)
Liver[a]	4.10[b,c] (0.60)	4.70[c] (0.62)	3.02[b,c] (0.64)	1.91[c] (0.68)	0.52[c] (0.12)
Kidneys[a]	9.28 (4.40)	3.54[b] (1.07)	3.80[c] (1.63)	3.26[c] (2.00)	0.87[b,c] (0.24)
Intestine[a]	0.76 (0.25)	1.04 (0.05)	1.52 (0.63)	2.14 (1.27)	0.13 (0.06)
Stomach[d]	0.69[c] (0.17)	0.53[c] (0.13)	0.54[c] (0.09)	0.42[c] (0.27)	0.36 (0.27)
Femur[a]	18.80[c] (3.59)	24.35[b,c](2.56)	25.25[b,c] (2.04)	22.74[c] (3.33)	24.80[c] (2.41)
^{186}Re-MAMA-BP					
Blood[a]	4.28[c] (0.38)	0.61 (0.19)	0.23[c] (0.04)	0.11[c] (0.04)	0.03 (0.01)
Liver[a]	5.66[c] (1.19)	4.19[c] (0.52)	2.25[c] (0.34)	1.31[c] (0.42)	0.71[c] (0.20)
Kidneys[a]	14.05[c] (3.51)	6.33[c] (2.06)	4.50[c] (0.53)	3.54[c] (0.73)	2.43[c] (0.53)
Intestine[a]	0.99 (0.18)	1.14 (0.12)	1.50 (0.09)	1.68 (1.52)	0.24 (0.14)
Stomach[d]	0.75 (0.25)	0.87[c] (0.26)	0.79[c] (0.15)	0.29[c] (0.08)	0.19 (0.04)
Femur[a]	16.41[c] (1.85)	20.07[c] (1.82)	19.78 (1.37)	20.86[c] (2.06)	21.38[c] (3.83)
^{186}Re-HEDP					
Blood[a]	2.70 (0.11)	0.62 (0.22)	0.41 (0.06)	0.27 (0.02)	0.04 (0.01)
Liver[a]	1.01 (0.16)	0.43 (0.22)	0.45 (0.15)	0.34 (0.10)	0.08 (0.01)
Kidneys[a]	7.92 (2.62)	2.24 (1.18)	1.37 (0.33)	1.02 (0.17)	0.42 (0.10)
Intestine[a]	0.64 (0.07)	0.92 (0.41)	1.34 (1.24)	2.13 (1.37)	0.37 (0.36)
Stomach[d]	1.26 (0.43)	2.72 (1.64)	2.54 (1.49)	1.17 (0.41)	0.57 (0.39)
Femur[a]	11.37 (1.23)	14.63 (2.60)	16.65 (3.16)	15.51 (4.00)	13.09 (2.90)

Each value represents the mean (S.D.) for five or six animals.
Significance was determined with the Tukey–Kramer test ($P<.05$).
[a] Expressed as percent injected dose per gram.
[b] Significantly different from ^{186}Re-MAMA-BP.
[c] Significantly different from ^{186}Re-HEDP.
[d] Expressed as percent injected dose.

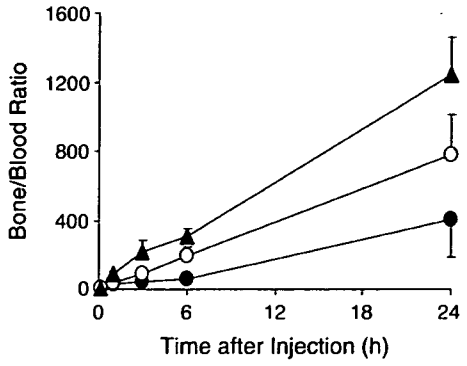

Fig. 2. Femur/blood ratios of radioactivity after the injection of ^{186}Re-MAMA-HBP (closed triangles), ^{186}Re-MAMA-BP (open circles) and ^{186}Re-HEDP (closed circles) in mice. Each value represents the mean± S.D. for five or six animals.

group was coupled with the active ester of the Tr-MAMA derivative **(2)**. Due to the insolubility of the bisphosphonate derivative **(3)** in organic solvents and the insolubility of the Tr-MAMA derivative **(2)** in aqueous solvents, the coupling reaction was performed in a solvent mixed with acetonitrile and water. However, the reaction did not proceed because the bisphosphonate derivative was deposited in the solvent during the mixing step. When triethylamine was added to the reaction mixture, the bisphosphonate derivative was soluble. This allowed the reaction to proceed. As a result, Tr-MAMA-HBP could be obtained. ^{186}Re-MAMA-HBP was prepared by complexation with ^{186}Re using citrate/$SnCl_2$ as a reducing system, just after the Tr groups of Tr-MAMA-HBP were deprotected by treatment with TFA and triethylsilane. The radiochemical yield of ^{186}Re-MAMA-HBP was 54%. After

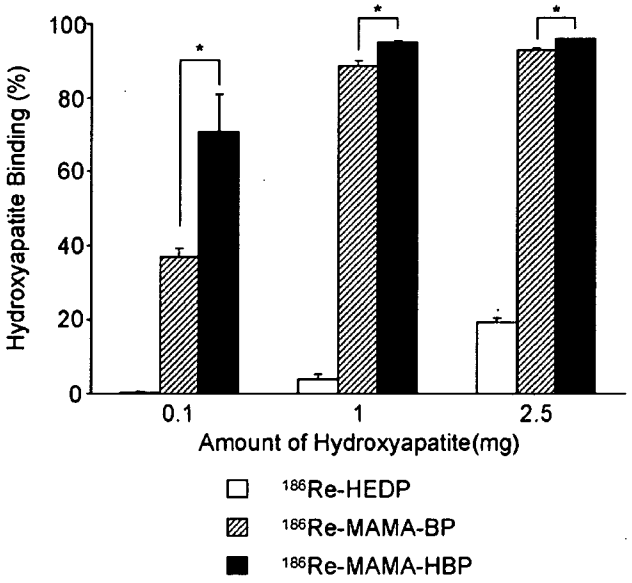

Fig. 3. Hydroxyapatite binding of ^{186}Re-labeled compounds. Each value represents the mean±S.D. for three samples. Significance was determined by unpaired Student's t test (*P<.05).

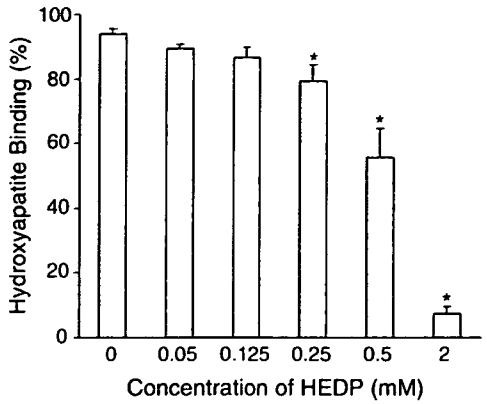

Fig. 4. Hydroxyapatite binding of ^{186}Re-MAMA-HBP and the inhibition of this binding by bisphosphonate (HEDP). Each value represents the mean±S.D. for three to six samples. The significance of differences was determined with a one-way analysis of variance followed by Dunnett's post hoc test, compared to samples without HEDP (*P<.05).

HPLC purification, ^{186}Re-MAMA-HBP had a radiochemical purity of over 95%. The radiochemical purity of both ^{186}Re-MAMA-BP and ^{186}Re-HEDP exceeded 95%.

3.2. In vitro stability

Table 1 shows the stability of ^{186}Re-MAMA-HBP in phosphate buffer. After 24 h of incubation, about 76% of ^{186}Re-MAMA-HBP remained intact. Under the same conditions, ^{186}Re-MAMA-BP showed stability similar to that of ^{186}Re-MAMA-HBP, whereas less than 30% of ^{186}Re-HEDP was intact [13].

3.3. Biodistribution experiments

The biodistribution of radioactivity after the intravenous injection of ^{186}Re-MAMA-HBP, ^{186}Re-MAMA-BP and ^{186}Re-HEDP in normal mice is summarized in Table 2. The tissue distribution of the radioactivity of ^{186}Re-MAMA-HBP was similar to that of ^{186}Re-MAMA-BP. ^{186}Re-MAMA-HBP, compared with ^{186}Re-MAMA-BP, showed a higher level in the femur and a faster blood clearance of radioactivity. Consequently, the femur/blood ratios of radioactivity were significantly higher after the administra-

Table 3
Absorbed dose estimates of ^{186}Re-MAMA-HBP, ^{186}Re-MAMA-BP and ^{186}Re-HEDP

Organ	^{186}Re-MAMA-HBP	^{186}Re-MAMA-BP	^{186}Re-HEDP
Bone surface[a]	6.13	5.71	2.02
Red marrow[a]	2.62	2.44	0.87
Liver[a]	0.08	0.09	0.01
Kidneys[a]	0.19	0.47	0.08
Small intestine[a]	0.10	0.08	0.10
Stomach[a]	0.09	0.05	0.14
Total body[a]	0.30	0.29	0.10
Effective dose[b]	0.46	0.42	0.19

[a] Expressed as milligrays per megabecquerel.
[b] Expressed as millisieverts per megabecquerel.

Table 4
Ratios of absorbed dose estimates between some organs and the bone surface

Organ	^{186}Re-MAMA-HBP	^{186}Re-MAMA-BP	^{186}Re-HEDP
Red marrow/ bone surface	0.427	0.427	0.431
Liver/ bone surface	0.013	0.016	0.005
Kidneys/ bone surface	0.031	0.082	0.040
Small intestine/ bone surface	0.016	0.014	0.050
Stomach/ bone surface	0.015	0.009	0.069
Total body/bone surface	0.049	0.051	0.050
Effective dose/ bone surface[a]	0.075	0.074	0.094

[a] Expressed as sieverts per gray.

tion of ^{186}Re-MAMA-HBP than after the administration of ^{186}Re-MAMA-BP (Fig. 2).

While ^{186}Re-HEDP also showed rapid accumulation and long retention in the femur, ^{186}Re-HEDP exhibited a significantly lower level of accumulation in the femur than ^{186}Re-MAMA-conjugated bisphosphonate derivatives (^{186}Re-MAMA-HBP and ^{186}Re-MAMA-BP). The blood clearance of ^{186}Re-HEDP was slower than that of ^{186}Re-MAMA-conjugated bisphosphonate derivatives. As a result, ^{186}Re-HEDP showed significantly lower femur/blood ratios of radioactivity (Fig. 2). Gastric accumulation of radioactivity after the administration of ^{186}Re-HEDP was higher, while hepatic and renal levels were lower than those of ^{186}Re-MAMA-conjugated bisphosphonate derivatives.

3.4. Hydroxyapatite binding assay

Fig. 3 shows the proportion of ^{186}Re-MAMA-BP, ^{186}Re-MAMA-HBP and ^{186}Re-HEDP that are bound to hydroxyapatite beads. With an increase in the amount of hydroxyapatite, the percentage of ^{186}Re-MAMA-BP, ^{186}Re-MAMA-HBP and ^{186}Re-HEDP that are bound to hydroxyapatite rose, and ^{186}Re-MAMA-HBP showed a significant increase compared with ^{186}Re-MAMA-BP. The binding affinity of ^{186}Re-HEDP to hydroxyapatite was much lower than that of ^{186}Re-MAMA-conjugated bisphosphonate, although strict comparison is difficult because of the difference in the concentrations of the ligand (bisphosphonate).

On the other hand, $^{186}ReO_4^-$ and ^{186}Re-MAMA hardly bound at all to hydroxyapatite beads (data not shown). The binding of ^{186}Re-MAMA-HBP was inhibited by the addition of a bisphosphonate compound (HEDP) in a concentration-dependent fashion (Fig. 4). These results indicated that the binding of ^{186}Re-MAMA-HBP to hydroxyapatite can be attributed to the character of the bisphosphonate site.

3.5. Partition coefficient

The log PC values of ^{186}Re-MAMA-BP and ^{186}Re-MAMA-HBP were much the same (-0.96 ± 0.01 vs. -1.02 ± 0.01), whereas ^{186}Re-HEDP had a lower log PC value (-1.54 ± 0.02).

3.6. Dosimetry

Table 3 shows absorbed radiation dose estimates for ^{186}Re-HEDP, ^{186}Re-MAMA-BP and ^{186}Re-MAMA-HBP. The radiation dose estimates for ^{186}Re-HEDP obtained in this study show similarity to those calculated from baboon data in van Aswegen et al. [20]. Table 4 shows the ratios of absorbed dose estimates between some organs and the bone surface. Since the bone surface is the target of internal radionuclide therapy, in obtaining an equal therapeutic effect, these ratios can be regarded as indices to unnecessary radiation. The red-marrow/bone-surface and total-body/bone-surface absorbed dose ratios are almost same among three compounds, and the effective-dose/bone-surface ratios of ^{186}Re-MAMA-BP and ^{186}Re-MAMA-HBP are lower than that of ^{186}Re-HEDP.

4. Discussion

The basic requirements for the effective use of radiopharmaceuticals in internal radiotherapy for the palliation of metastatic bone pain include extensive accumulation in the bone following peripheral administration.

Bisphosphonates have been used widely as inhibitors of bone resorption for the treatment of bone diseases and have been investigated extensively [21,22]. All bisphosphonates contain two phosphonate groups attached to a single carbon atom, forming a P–C–P structure; this central carbon has various side chains. Among these compounds, bisphosphonates containing a hydroxy group at the central carbon have been reported to have a higher affinity for bone minerals [14,15]. In addition, in the case of metal complexes, it was also reported that the cobalt (III) hydroxymethylene diphosphonate (HMDP) complex had a higher affinity for calcium than the cobalt (III) methylene diphosphonate (MDP) complex [23]. Furthermore, in the case of radiopharmaceuticals, it was also reported that ^{99m}Tc-HMDP, compared with ^{99m}Tc-MDP, demonstrated a higher uptake in bones [24,25]. Thus, based on the concept of bifunctional radiopharmaceuticals, we synthesized ^{186}Re-MAMA-HBP, a compound with a stable ^{186}Re-MAMA chelate moiety attached to a bisphosphonate derivative containing a hydroxy group at the central carbon. As expected, ^{186}Re-MAMA-HBP showed greater affinity for bone minerals (hydroxyapatite) compared with ^{186}Re-MAMA-BP, a bisphosphonate derivative without a hydroxy group at the central carbon (Fig. 3). This characteristic was reflected in its behavior in vivo. Namely, in biodistribution experiments, more ^{186}Re-MAMA-HBP than ^{186}Re-MAMA-BP accumulated in the femur (Table 2). These findings suggest that a hydroxyl group at the central carbon in the design of a ^{186}Re-chelate-conjugated bisphosphonate derivative is effective in enhancing accumulation in bones. Furthermore, ^{186}Re-MAMA-HBP showed higher accumulation in the femur, a

lower level in the stomach and more rapid clearance from the blood than ^{186}Re-HEDP (Table 2). These findings indicated high affinity for bone and good stability in vivo, reflecting the results of experiments in vitro (Fig. 3, Table 1). These results demonstrate that MAMA moiety is useful as a chelating group in forming a stable complex with ^{186}Re in a bifunctional radiopharmaceutical containing bisphosphonate as a biologically active molecule.

We expected that these results would lead to a decrease in the level of unnecessary radiation. Certainly, the radiation dose of ^{186}Re-MAMA-HBP for the stomach decreased, compared with ^{186}Re-HEDP. However, in the case of radiation dose for the bone marrow, known as the dose-limiting factor of bone-seeking agents, the absorbed dose ratio between the bone marrow and the bone surface of ^{186}Re-MAMA-HBP was equivalent to that of ^{186}Re-HEDP. The slight improvement of blood clearance should contribute little to the radiation dose for the bone marrow because the radiation dose for the bone marrow is highly influenced by the accumulation of radioactivity in the bone.

The radiation dose of ^{186}Re-MAMA-HBP for the liver increased, compared with ^{186}Re-HEDP, because hepatic radioactivity levels were significantly higher after the administration of ^{186}Re-MAMA-HBP than after the administration of ^{186}Re-HEDP. Since ^{186}Re-MAMA-HBP was more lipophilic than ^{186}Re-HEDP, as evident from the partition coefficient (1-octanol/phosphate buffer, pH 7.4), extensive hepatic uptake of ^{186}Re-MAMA-HBP may be caused by increase in lipophilicity.

When bone affinity is compared with those of other bone-seeking agents measured in different species, uptake value is expressed as percent dose per gram of tissue times body weight, in order to normalize the difference in the weight of animals. The corresponding value of ^{186}Re-MAMA-HBP in the femur 1 h after injection was 694%. ^{153}Sm-ethylene diamine tetramethylene phosphonate (EDTMP) was approved by the Food and Drug Administration for the treatment of painful bone metastases in 1997, and the uptake value was 707% (2 h in rats) [26]. Since the uptake value of ^{186}Re-MAMA-HBP is comparable to that of ^{153}Sm-EDTMP, it is expected that ^{186}Re-MAMA-HBP will be of clinical use from the point of view of bone uptake. However, the nonosseous tissue clearance of ^{186}Re-MAMA-HBP must not be rapid as that of ^{153}Sm-EDTMP because it was reported that ^{99m}Tc-MDP and ^{153}Sm-EDTMP showed no significant soft tissue uptake [27].

In conclusion, based on the idea of bifunctional radiopharmaceuticals, we developed a ^{186}Re complex-conjugated bisphosphonate derivative with a hydroxy group, ^{186}Re-MAMA-HBP. When administered to mice, ^{186}Re-MAMA-HBP showed greater affinity for bones and much higher femur/blood ratios of radioactivity than either ^{186}Re-HEDP or ^{186}Re-MAMA-BP. These findings should provide useful information on the drug design of bone-seeking therapeutic radiopharmaceuticals.

Acknowledgments

This work was supported, in part, by Grants-in-Aid for Scientific Research from the Ministry of Education, Culture, Sports, Science and Technology of Japan and a research grant from the Sagawa Foundation for the Promotion of Cancer Research.

References

[1] Yoneda T, Sasaki A, Mundy GR. Osteolytic bone metastasis in breast cancer. Breast Cancer Res Treat 1994;32:73–84.
[2] Mercadante S. Malignant bone pain: pathophysiology and treatment. Pain 1997;69:1–18.
[3] Uppelschoten JM, Wanders SL, de Jong JM. Single-dose radiotherapy (6 Gy): palliation in painful bone metastases. Radiother Oncol 1995;36:198–202.
[4] Pandit-Taskar N, Batraki M, Divgi CR. Radiopharmaceutical therapy for palliation of bone pain from osseous metastases. J Nucl Med 2004; 45:1358–65.
[5] McEwan AJ. Use of radionuclides for the palliation of bone metastases. Semin Radiat Oncol 2000;10:103–14.
[6] Elder RC, Yuan J, Helmer B, Pipes D, Deutsch K, Deutsch E. Studies of the structure and composition of rhenium-1,1-hydroxyethylidene-diphosphonate (HEDP) analogues of the radiotherapeutic agent (186)ReHEDP. Inorg Chem 1997;36:3055–63.
[7] Kolesnikov-Gauthier H, Carpentier P, Depreux P, Vennin P, Caty A, Sulman C. Evaluation of toxicity and efficacy of ^{186}Re-hydroxyethylidene diphosphonate in patients with painful bone metastases of prostate or breast cancer. J Nucl Med 2000;41:1689–94.
[8] Limouris GS, Shukla SK, Condi-Paphiti A, Gennatas C, Kouvaris I, Vitoratos N, et al. Palliative therapy using rhenium-186-HEDP in painful breast osseous metastases. Anticancer Res 1997;17: 1767–72.
[9] O'Sullivan JM, McCready VR, Flux G, Norman AR, Buffa FM, Chittenden S, et al. High activity rhenium-186 HEDP with autologous peripheral blood stem cell rescue: a phase I study in progressive hormone refractory prostate cancer metastatic to bone. Br J Cancer 2002;86:1715–20.
[10] De Winter F, Brans B, Van De Wiele C, Dierckx RA. Visualization of the stomach on rhenium-186 HEDP imaging after therapy for metastasized prostate carcinoma. Clin Nucl Med 1999;24:898–9.
[11] de Klerk JM, van Dijk A, van het Schip AD, Zonnenberg BA, van Rijk PP. Pharmacokinetics of rhenium-186 after administration of rhenium-186-HEDP to patients with bone metastases. J Nucl Med 1992;33:646–51.
[12] Arano Y, Ono M, Wakisaka K, Uezono T, Akizawa H, Motonari Y, et al. Synthesis and biodistribution studies of ^{186}Re complex of 1-hydroxyethylidene-1,1-diphosphonate for treatment of painful osseous metastases. Radioisotopes 1995;44:514–22.
[13] Ogawa K, Mukai T, Arano Y, Hanaoka H, Hashimoto K, Nishimura H, et al. Design of a radiopharmaceutical for the palliation of painful bone metastases: rhenium-186-labeled bisphosphonate derivative. J Label Cmpd Radiopharm 2004;47:753–61.
[14] Meyer JL, Nancollas GH. The influence of multidentate organic phosphonates on the crystal growth of hydroxyapatite. Calcif Tissue Res 1973;13:295–303.
[15] van Beek E, Hoekstra M, van de Ruit M, Lowik C, Papapoulos S. Structural requirements for bisphosphonate actions in vitro. J Bone Miner Res 1994;9:1875–82.
[16] Kobayashi K, Motoishi S, Terunuma K, Rauf AA, Hashimoto K. Production of $^{186/188}$Re and recovery of tungsten from spent ^{188}W/^{188}Re generator. Radiochemistry 2000;42:551–4.
[17] Kieczykowski GR. New process for preparing an antihypercalcemic agent. UK Patent GB 2248061A, 1992.

[18] Kasugai S, Fujisawa R, Waki Y, Miyamoto K, Ohya K. Selective drug delivery system to bone: small peptide $(Asp)_6$ conjugation. J Bone Miner Res 2000;15:936–43.

[19] Fujisawa R, Kuboki Y. Preferential adsorption of dentin and bone acidic proteins on the (100) face of hydroxyapatite crystals. Biochim Biophys Acta 1991;1075:56–60.

[20] van Aswegen A, Roodt A, Marais J, Botha JM, Naude H, Lotter MG, et al. Radiation dose estimates of ^{186}Re-hydroxyethylidene diphosphonate for palliation of metastatic osseous lesions: an animal model study. Nucl Med Commun 1997;18:582–8.

[21] Fleisch H. Bisphosphonates: mechanisms of action. Endocr Rev 1998;19:80–100.

[22] Rodan GA, Fleisch HA. Bisphosphonates: mechanisms of action. J Clin Invest 1996;97:2692–6.

[23] Jurisson SS, Benedict JJ, Elder RC, Whittle R, Deutsch E. Calcium affinity of coordinated diphosphonate ligands. Single-crystal structure of $[(en)_2Co(O_2P(OH)CH_2P(OH)O_2]ClO_4 \cdot H_2O$. Implications for the chemistry of technetium-99m-diphosphonate skeletal imaging agents. Inorg Chem 1983;22:1332–8.

[24] Subramanian G, McAfee JG, Thomas FD, Feld TA, Zapf-Longo C, Palladino E. New diphosphonate compounds for skeletal imaging: comparison with methylene diphosphonate. Radiology 1983;149: 823–8.

[25] Fogelman I, Pearson DW, Bessent RG, Tofe AJ, Francis MD. A comparison of skeletal uptakes of three diphosphonates by whole-body retention: concise communication. J Nucl Med 1981; 22:880–3.

[26] Goeckeler WF, Edwards B, Volkert WA, Holmes RA, Simon J, Wilson D. Skeletal localization of samarium-153 chelates: potential therapeutic bone agents. J Nucl Med 1987;28:495–504.

[27] Ketring AR. ^{153}Sm-EDTMP and ^{186}Re-HEDP as bone therapeutic radiopharmaceuticals. Int J Rad Appl Instrum B 1987;14:223–32.

Available online at www.sciencedirect.com
SCIENCE DIRECT
Nuclear Medicine and Biology 33 (2006) 489–494
NUCLEAR MEDICINE — AND — BIOLOGY
www.elsevier.com/locate/nucmedbio

Development of a ^{111}In-labeled peptide derivative targeting a chemokine receptor, CXCR4, for imaging tumors

Hirofumi Hanaoka[a,b], Takahiro Mukai[c,d], Hirokazu Tamamura[a,e], Tomohiko Mori[c], Seigo Ishino[a], Kazuma Ogawa[a], Yasuhiko Iida[b], Ryuichiro Doi[c], Nobutaka Fujii[a], Hideo Saji[a,*]

[a]*Graduate School of Pharmaceutical Sciences, Kyoto University, Yoshida Shimoadachi-cho, Sakyo-ku, Kyoto 606-8501, Japan*
[b]*Graduate School of Medicine, Gunma University, Showa-machi, Maebashi 371-8511, Japan*
[c]*Graduate School of Medicine, Kyoto University, Shogoin Kawahara-cho, Sakyo-ku, Kyoto 606-8507, Japan*
[d]*Graduate School of Pharmaceutical Sciences, Kyushu University, Maidashi, Higashi-ku, Fukuoka 812-8582, Japan*
[e]*Institute of Biomaterials and Bioengineering, Tokyo Medical and Dental University, Chiyoda-ku, Tokyo 101-0062, Japan*

Received 7 October 2005; received in revised form 12 January 2006; accepted 12 January 2006

Abstract

The chemokine receptor CXCR4 is highly expressed in tumor cells and plays an important role in tumor metastasis. The aim of this study was to develop a radiopharmaceutical for the imaging of CXCR4-expressing tumors in vivo. Based on structure–activity relationships, we designed a 14-residue peptidic CXCR4 inhibitor, Ac-TZ14011, as a precursor for radiolabeled peptides. For ^{111}In-labeling, diethylenetriaminepentaacetic acid (DTPA) was attached to the side chain of D-Lys^{8} which is distant from the residues indispensable for the antagonistic activity. In-DTPA-Ac-TZ14011 inhibited the binding of a natural ligand, stromal cell-derived factor-1α, to CXCR4 in a concentration-dependent manner with an IC_{50} of 7.9 nM (Ac-TZ14011: 1.2 nM). In biodistribution experiments, more ^{111}In-DTPA-Ac-TZ14011 accumulated in the CXCR4-expressing tumor than in blood or muscle. Furthermore, the tumor-to-blood and tumor-to-muscle ratios were significantly reduced by coinjection of Ac-TZ14011, indicating a CXCR4-mediated accumulation in tumor. These findings suggested that ^{111}In-DTPA-Ac-TZ14011 would be a potential agent for the imaging of CXCR4 expression in metastatic tumors in vivo.

Keywords: CXCR4; Peptide radiopharmaceutical; Indium-111; Metastatic tumor

1. Introduction

Chemokines are a family of small proteins (8–14 kDa) that chemoattract leukocytes by binding to cell surface receptors, chemokine receptors [1]. The chemokine receptor family, which belongs to a superfamily of seven transmembrane domain G-protein-coupled receptors, comprises 18 members [2]. In 1996, one member, CXCR4, was identified as a coreceptor for the entry of T-cell line-tropic HIV-1 [3]. Since then, this receptor has attracted considerable attention as a pathogenic factor or a therapeutic target for HIV infection. Recent studies indicated that CXCR4 and its ligand, stromal cell-derived factor-1 (SDF-1), play an important role also in tumor metastasis [4–8]. Müller et al. [4] reported that CXCR4 was highly expressed in breast cancer and SDF-1 was highly expressed in organs representing the first destinations of metastasis. Moreover, they demonstrated that neutralization with anti-CXCR4 monoclonal antibody significantly inhibited the metastasis of breast cancer cells in mice. Similar results were obtained in other types of cancer [5–8]. These findings suggest that CXCR4 is a potential target for the in vivo imaging of metastatic tumors.

We have previously demonstrated that a peptide with anti-HIV-1 activity, T22 ([Tyr^{5,12}, Lys^{7}]-polyphemusin II), is an inhibitor of CXCR4 that blocks the entry of T-cell line-tropic HIV-1 mediated by this receptor. T22 is an 18-residue peptide amide, which was previously found by us based on an analysis of the structure–activity relationships of self-defense peptides of horseshoe crabs, tachyplesin and polyphemusin [9,10]. On the basis of the structure of T22, we designed and synthesized several downsized analogs, 14-residue peptides [11,12]. Among them, T140 showed the greatest inhibitory effect on the binding of an anti-CXCR4 monoclonal antibody to CXCR4 and the strongest inhibitory

* Corresponding author. Tel.: +81 75 753 4556; fax: +81 75 753 4568.
E-mail address: hsaji@pharm.kyoto-u.ac.jp (H. Saji).

0969-8051/$ – see front matter © 2006 Elsevier Inc. All rights reserved.
doi:10.1016/j.nucmedbio.2006.01.006

activity against HIV-1 entry [12]. The aim of this study was to develop a radiolabeled T140 derivative as an imaging agent for metastatic tumors. Considering that the three residues on the restricted backbone (L-3-(2-naphthyl)alanine (Nal)[3], Tyr^5 and Arg^{14}) and the single residue in the flexible region (Arg^2) form the intrinsic pharmacophore of T140 [13–15], we designed a 14-residue peptidic inhibitor, Ac-TZ14011, as the precursor for radiolabeled peptides (Fig. 1). This precursor contains the above four residues which are necessary for the inhibitory activity against CXCR4. Furthermore, for site-selective conjugation of radiolabels, Ac-TZ14011 has a single amino group (D-Lys^8), which is distant from the pharmacophore, and the carboxyl group of Arg^{14} of Ac-TZ14011 is protected via amidation for stability in vivo [16,17].

^{111}In constitutes one of the most useful radionuclides for the radiolabeling of peptides for diagnostic applications in nuclear medicine. Diethylenetriaminepentaacetic acid (DTPA) is still an attractive chelating agent with which to prepare ^{111}In-labeled peptides since it provides ^{111}In-labeled peptides with highly specific activity. In addition, the development of a monoreactive DTPA derivative has provided an easy and efficient way to prepare DTPA-conjugated peptides [18,19]. In this study, DTPA-Ac-TZ14011 was prepared using a monoreactive DTPA derivative and coordinated with nonradioactive In or radioactive ^{111}In. Furthermore, the antagonistic activity of In-DTPA-Ac-TZ14011 and in vivo behavior of ^{111}In-DTPA-Ac-TZ14011 were investigated and the applicability of ^{111}In-DTPA-Ac-TZ14011 as a radiopharmaceutical for imaging tumors was evaluated.

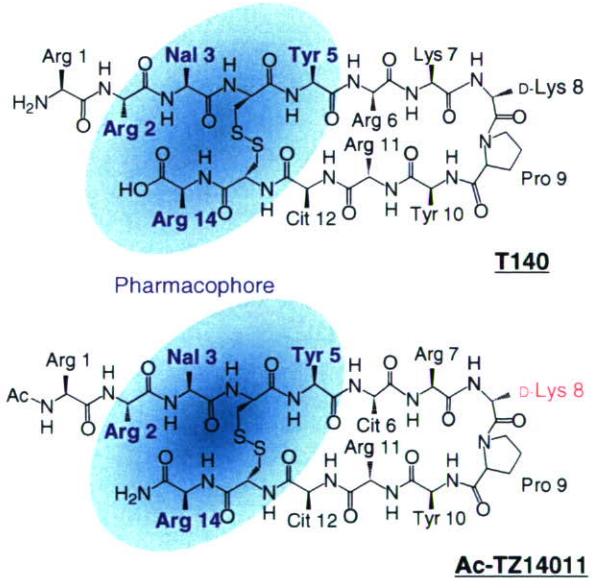

Fig. 1. Structures of T140 and Ac-TZ14011. There are four amino acid residues indispensable for the antagonistic activity (blue residues) which formed the pharmacophore. Nal: L-3-(2-naphthyl)alanine, Cit: L-citrulline. Ac-TZ14011 has a single amino group (D-Lys^8) for site-selective conjugation of radiolabels, which is distant from the pharmacophore.

2. Materials and methods

2.1. Reagents and chemicals

$^{111}InCl_3$ (74 MBq/ml in 0.02N HCl) was kindly supplied by Nihon Medi-Physics (Nishinomiya, Japan). 9-Fluorenylmethoxycarbonyl (Fmoc)-protected amino acids and 4-(2′,4′-dimethoxyphenylaminomethyl)phenoxy (SAL) resin were purchased from Watanabe Chemical Industries (Hiroshima, Japan) or Calbiochem-Novabiochem Japan (Tokyo, Japan). 1-*tert*-Butyl hydrogen 3,6,9-tris((*tert*-butoxycarbonyl)methyl)-3,6,9-triazaundecanedioic acid (mDTPA) was synthesized as reported previously [18]. All the other chemicals were purchased from either Nacalai Tesque (Kyoto, Japan) or Wako Pure Chemical Industries (Osaka, Japan). Ion spray mass spectra (IS-MS) were obtained with the API III model (PerkinElmer Sciex Instruments, Thornhill, Canada). Cellulose acetate electrophoresis (CAE) strips were run in veronal buffer (pH 8.6, I=0.06) at a constant current of 0.8 mA for 40 min. Thin-layer chromatography (TLC) analyses were performed with silica plates (Silica gel 60, Merck, Darmstadt, Germany) with 10% aqueous ammonium chloride–methanol (1:1) as the developing solvent.

2.2. Synthesis of In-DTPA-Ac-TZ14011

Fig. 2 shows the scheme for the synthesis of In-DTPA-Ac-TZ14011. A protected peptide was constructed using Fmoc-based solid-phase synthesis on SAL resin and its N-terminus was acetylated. After being treated with thioanisole/trifluoroacetic acid (TFA) in the presence of *m*-cresol and 1,2-ethanedithiol, the crude peptide was air-oxidized and purified by reversed-phase HPLC (RP-HPLC). RP-HPLC was carried out with a Cosmosil 5C18-AR column (20×250 mm, Nacarai Tesque) eluted with a linear gradient of 10–30% acetonitrile in 0.1% aqueous TFA in 30 min at a flow rate of 7 ml/min. Fractions containing the peptide were collected, and the solvent was removed by lyophilization to afford Ac-TZ14011 as a white powder. IS-MS calcd for $C_{92}H_{144}N_{35}O_{19}S_2$ [M+H$^+$]: *m/z* 2107.1, found: *m/z* 2107.4.

DTPA-Ac-TZ14011 was prepared by mDTPA conjugation. Briefly, to a solution of mDTPA (19 mg, 30.8 μmol) in acetonitrile (350 μl) were added *N*-hydroxysuccinimide (3.74 mg, 32.3 μmol) and *N*,*N*-dicyclohexylcarbodiimide (6.67 mg, 32.3 μmol) at 0°C, and the mixture was incubated overnight at room temperature. After cooling to 0°C again, 200 μl of Ac-TZ14011 (10.2 mg, 3.65 μmol) in a mixture of acetonitrile and phosphate-buffered saline (pH 7.4) (1:1) was added to the reaction mixture and incubated overnight at room temperature. After treatment with 95% TFA, the crude peptide was purified by RP-HPLC under the same conditions as above. IS-MS calcd for $C_{106}H_{165}N_{38}O_{28}S_2$ [M+H$^+$]: *m/z* 2482.2, found: *m/z* 2482.9.

Fifty microliters of DTPA-Ac-TZ14011 (610 μg, 0.20 μmol) in 0.1 M acetic acid was reacted with 25 μl of nonradioactive $InCl_3 \cdot 4H_2O$ (64.5 μg, 0.22 μmol) in 0.02N HCl for 30 min at room temperature. Subsequent

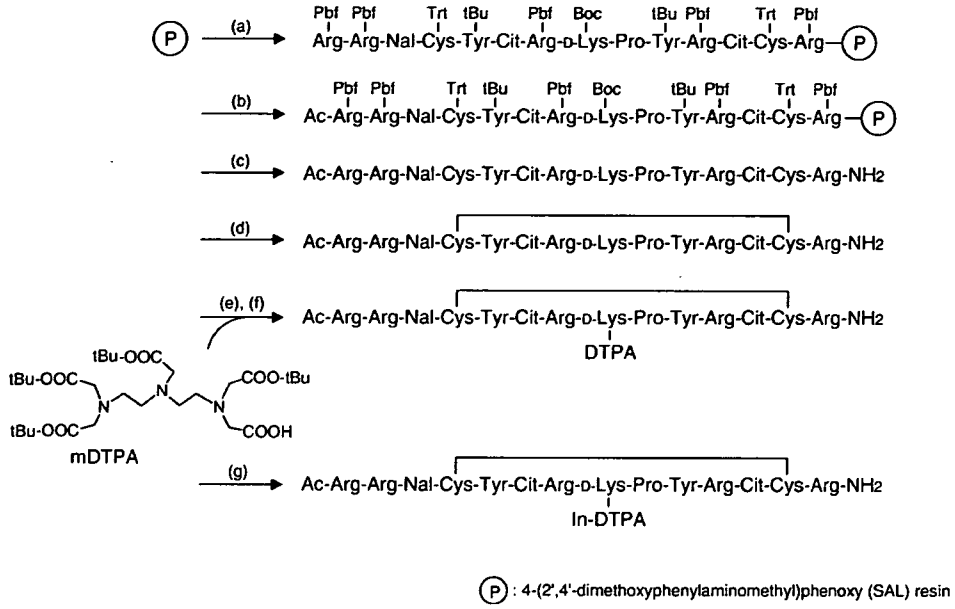

Fig. 2. Synthesis of In-DTPA-Ac-TZ14011. Reagents: (a) stepwise elongation; (b) acetic anhydride, pyridine; (c) trifluoroacetic acid, thioanisole, *m*-cresol, 1,2-ethanedithiol; (d) air oxidation; (e) *N*-hydroxysuccinimide, *N,N*-dicyclohexylcarbodiimide; (f) trifluoroacetic acid; (g) $InCl_3 \cdot 4H_2O$.

purification by RP-HPLC was carried out with a Hydrosphere C18 column (4.6×250 mm, YMC, Kyoto, Japan) eluted with 17% acetonitrile in 0.1% aqueous TFA at a flow rate of 1 ml/min. Fractions containing the peptide were collected, and the solvent was removed by lyophilization to afford In-DTPA-Ac-TZ14011 as a white powder. IS-MS calcd for $InC_{106}H_{161}N_{38}O_{28}S_2$ $[M+H^+]$: *m/z* 2594.2, found: *m/z* 2594.3.

2.3. Synthesis of ^{111}In-DTPA-Ac-TZ14011

$^{111}InCl_3$ (3.7 MBq) in 0.02N HCl (100 μl) was added to DTPA-Ac-TZ14011 (10 μg) in 0.1 M acetic acid (200 μl), and the mixture was incubated for 30 min at room temperature. Then, ^{111}In-DTPA-Ac-TZ14011 was separated from DTPA-Ac-TZ14011 by RP-HPLC under the same conditions used for the purification of In-DTPA-Ac-TZ14011. The radiochemical purity of ^{111}In-DTPA-Ac-TZ14011 was determined by TLC, CAE and RP-HPLC.

2.4. Binding assay

The binding assay was performed according to the procedure of Hesselgesser et al. [20] with a slight modification. The stable CXCR4-transfected Chinese hamster ovary (CHO) cell lines were prepared by transfection with cDNA encoding alanine scanning mutants in pcDNA3 (Invitrogen, Carlsbad, CA, USA) using lipofectamine (GIBCO, Rockville, MD, USA) and selection in neomycin (G418 500 mg/ml; GIBCO). The expression of CXCR4 on the surface of each transfectant was measured by flow cytometry. CXCR4-transfected CHO cell lines were suspended in the binding buffer (Ham's F-12 containing 20 mM HEPES and 0.5% BSA) and placed in siliconized tubes (5×10^5 cells/120 μl/tube). Binding reactions were performed on ice for 1 h in the presence of $[^{125}I]$SDF-1α (PerkinElmer Life Sciences, Boston, MA, USA) and various concentrations of peptides. Cells were separated from the buffer by centrifugation through a dibutylphthalate/olive oil mixture. After removal of the water and oil layer, cell-associated radioactivity was measured. The 50% inhibitory concentration (IC_{50}) of peptides was determined based on inhibition of the binding of SDF-1α to CXCR4-transfected CHO cells.

2.5. Calcium fluorimetry

Calcium fluorimetry was performed as described previously [21]. CXCR4-transfected CHO cell lines were placed in wells of a microtiter tray (3×10^4 cells/100 μl/well) and incubated for 1 day at 37°C in a CO_2 incubator. The cells were loaded with 5 μM of Fura-2-AM (Dojindo Laboratories, Kumamoto, Japan), 2.5 mM probenecid (Sigma, St Louis, MO, USA) and 20 mM HEPES (pH 7.4) in Ham's F-12 (80 μl/well) for 1 h at 37°C. After the cells were incubated with various concentrations of T140 analogs for 3 min, recombinant human SDF-1α (PeproTech EC, London, UK) was added. Changes in intracellular Ca^{2+} concentrations were measured by a spectrofluorometer (96-well Fluorescence Drug Screening System, Hamamatsu Photonix, Hamamatsu, Japan) using a modified version of the Fura-2 method [22]. The IC_{50} of peptides was determined based on the inhibition of Ca^{2+} mobilization induced by SDF-1α through CXCR4.

2.6. Biodistribution study in tumor-bearing mice

Animal experiments were conducted in accordance with our institutional guidelines and were approved by the Kyoto University Animal Care Committee. Athymic nude BALB/c

mice (8 weeks old, female) were inoculated subcutaneously with CXCR4-expressing pancreatic carcinoma cells, AsPC-1 [23,24]. When tumors were approximately 0.5 cm in diameter, the animals were intravenously injected with ^{111}In-DTPA-Ac-TZ14011 (25–30 kBq). The biodistribution of radioactivity was monitored at 1, 6 and 24 h postinjection. Groups of five mice were used for the experiments. Organs of interest were excised and weighed, and the radioactivity counts were determined with a well counter (ARC380CL, Aloka, Tokyo, Japan). For the in vivo blocking experiment, mice were coinjected with Ac-TZ14011 (10 mg/kg).

2.7. Statistical analysis

Statistical analysis was performed by using the unpaired *t*-test. $P<.05$ was considered to be statistically significant.

3. Results and discussion

T140 and its analogs have one disulfide bond and maintain an antiparallel β-sheet structure connected by a type II′ β-turn with D-Lys^8-Pro^9 at the (*i*+1) and (*i*+2) positions, and the side chain of D-Lys^8 is distant from the pharmacophore for the antagonistic activity [14,15]. Therefore, we designed Ac-TZ14011 as a mother compound that contains the residues indispensable for the antagonistic activity and has a single amino group of D-Lys^8 for site-selective conjugation of DTPA (Fig. 1). In calcium fluorimetric assays, this compound showed strong inhibitory activity equal to that of T140 (Table 1). To assess the effect of the conjugation of In-DTPA with Ac-TZ14011 on the antagonistic activity toward CXCR4, nonradioactive In-DTPA-Ac-TZ14011 was synthesized (Fig. 2). In binding assays with CXCR4, In-DTPA-Ac-TZ14011 maintained strong inhibitory activity although its IC_{50} value was slightly larger than that of Ac-TZ14011 (Table 1). This result indicated the validity of the chemical design of In-DTPA-Ac-TZ14011 based on structure–activity relationships.

In RP-HPLC analyses, In-DTPA-Ac-TZ14011 and DTPA-Ac-TZ14011 showed well-separated peaks as shown in Fig. 3. After purification by RP-HPLC under the same conditions, ^{111}In-DTPA-Ac-TZ14011 was obtained with high radiochemical purity (over 96%) as determined by TLC, CAE and RP-HPLC. The radioactivity pharmacokinetics of ^{111}In-DTPA-Ac-TZ14011 was evaluated in nude mice bearing the CXCR4-expressing pancreatic carcinoma AsPC-1 (Table 2). ^{111}In-DTPA-Ac-TZ14011 showed a rapid clearance from the blood and a marked accumulation and retention in the liver, kidney and spleen. The accumulation of radioactivity was greater in the tumor than in the blood or muscle (Table 2). In mice, CXCR4 mRNA is highly expressed in various lymphoid tissues and cells such as spleen, thymus, lymph node, bone marrow and leukocytes [25,26]. Thus, since liver and spleen are concerned with the immune system, the accumulation of ^{111}In-DTPA-Ac-TZ14011 in these organs should be mediated by CXCR4-binding. In fact, coinjection of Ac-TZ14011 significantly reduced the accumulation in the liver by over one-tenth and in the spleen by over one-third. This marked reduction of radioactivity in the liver and spleen on the coinjection of Ac-TZ14011 caused the high levels of radioactivity in the blood and consequently increased the accumulation of radioactivity in organs which were small in size and/or did not take up much radioactivity (Table 2). The accumulation in the tumor was also increased by coinjection of Ac-TZ14011, but the tumor-to-blood and tumor-to-muscle ratios were significantly reduced (Table 2). Since there is very little or no CXCR4 in the muscle [26],

Table 1
Antagonistic activity of T140 derivatives

	IC_{50} (nM)	
	SDF-1α binding[a]	Ca^{2+} mobilization[b]
In-DTPA-Ac-TZ14011	7.9	ND[c]
Ac-TZ14011	1.2	2.6
T140	ND[c]	2.2

[a] Values are the concentrations for 50% inhibition of the binding of [^{125}I]SDF-1α to CXCR4.

[b] Values are the concentrations for 50% inhibition of Ca^{2+} mobilization induced by SDF-1á through CXCR4.

[c] Not determined.

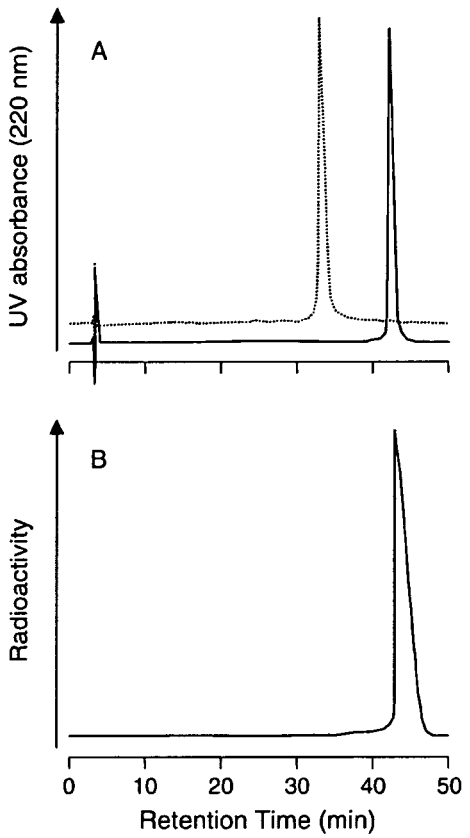

Fig. 3. Reversed-phase HPLC profiles of nonradioactive In-DTPA-Ac-TZ14011 (solid line), DTPA-Ac-TZ14011 (broken line) (A) and ^{111}In-DTPA-Ac-TZ14011 (B).

Table 2
Biodistribution of radioactivity after intravenous injection of ^{111}In-DTPA-Ac-TZ14011 in nude mice bearing pancreatic carcinoma, AsPC-1

	1 h	6 h	24 h	1 h+ Ac-TZ14011[a]
Blood[b]	0.39 (0.06)	0.05 (0.01)	0.03 (0.01)	2.06** (0.61)
Liver[b]	27.0 (2.9)	25.2 (2.0)	19.3 (2.5)	1.95** (0.25)
Kidney[b]	50.9 (4.3)	43.4 (6.3)	29.5 (5.7)	45.4 (6.8)
Spleen[b]	8.22 (0.70)	7.57 (0.54)	5.83 (0.99)	2.66** (1.21)
Pancreas[b]	0.15 (0.03)	0.05 (0.01)	0.05 (0.02)	1.07** (0.46)
Muscle[b]	0.17 (0.05)	0.07 (0.02)	0.07 (0.01)	1.35** (0.26)
Tumor[b]	0.51 (0.08)	0.20 (0.03)	0.14 (0.03)	1.70** (0.27)
T/B ratio[c]	1.31 (0.14)	4.05 (0.79)	5.65 (2.89)	0.88* (0.31)
T/M ratio[d]	3.17 (0.99)	4.43 (1.89)	3.23 (1.08)	1.31** (0.41)

Each value represents the mean (S.D.) for five animals.
[a] Coinjection with unlabeled Ac-TZ14011 (10 mg/kg).
[b] Expressed as % injected dose per gram.
[c] Tumor-to-blood ratio.
[d] Tumor-to-muscle ratio.
* $P<.05$, comparison between ^{111}In-DTPA-Ac-TZ14011 with or without unlabeled Ac-TZ14011 at 1 h.
** $P<.005$, comparison between ^{111}In-DTPA-Ac-TZ14011 with or without unlabeled Ac-TZ14011 at 1 h.

tumor-to-muscle ratios reflect target-to-nontarget ratios. Thus, the reduction in the tumor-to-muscle ratio caused by the coinjection of Ac-TZ14011 indicated that ^{111}In-DTPA-Ac-TZ14011 accumulated in the tumor through CXCR4. On the other hand, coinjection of Ac-TZ14011 did not alter the levels of ^{111}In-DTPA-Ac-TZ14011 in the kidney, suggesting a nonspecific accumulation. This is consistent with previous findings that CXCR4 mRNA levels expressed in the kidney were very low [25,26]. Recent studies indicated that an electrostatic interaction between positively charged peptides and the negatively charged surface of renal proximal tubular cells plays an important role in the reabsorption of peptides into proximal tubular cells [27–29]. Since five Arg residues are contained in the peptide ^{111}In-DTPA-Ac-TZ14011, the highly positive charge would cause a greater nonspecific accumulation in the kidney even compared to other ^{111}In-DTPA peptides [28,30,31]. Due to its accumulation in nontarget organs, ^{111}In-DTPA-Ac-TZ14011 may be unavailable as a radiopharmaceutical for screening small tumors, particularly in the kidneys and their surroundings.

It was reported that CXCR4 expression could be a powerful predictive factor for prognosis (recurrence, metastasis or survival rate) in colorectal cancer [32,33], malignant melanoma [34] and osteosarcoma [35]. Therefore, a CXCR4 imaging agent would be a new type of radiopharmaceutical for predicting the prognosis of cancer patients. CXCR4 also represents a novel target for tumor therapy, and some CXCR4 inhibitors have been investigated as anti-metastatic agents [36–39]. These agents showed positive effects in suppressing tumor metastasis; however, they would also have deleterious effects on normal physiological functions since CXCR4 plays a crucial role in numerous biological processes [2]. Therefore, in vivo imaging of CXCR4 expression could be a potential method for determining the dose of anti-metastatic agents and for monitoring their therapeutic efficacy.

In conclusion, we designed ^{111}In-DTPA-Ac-TZ14011 based on the structure–activity relationships of peptidic CXCR4 inhibitors. In-DTPA-Ac-TZ14011 showed strong inhibitory activity against the binding of CXCR4 to an endogenous ligand. Furthermore, the accumulation of ^{111}In-DTPA-Ac-TZ14011 in the CXCR4-expressing tumor was greater than that in the blood or muscle, being mediated by this receptor. These findings suggest that ^{111}In-DTPA-Ac-TZ14011 is a potential radiopharmaceutical for the imaging of CXCR4 expression in metastatic tumors in vivo for predicting the prognosis of cancer patients and for monitoring the therapeutic efficacy of anti-metastatic agents.

Acknowledgments

We are grateful to Nihon Medi-Physics (Nishinomiya, Japan) for the gift of $^{111}InCl_3$. This work was supported in part by a Grant-in-Aid for Cancer Research from the Ministry of Health, Labour and Welfare.

References

[1] Zlotnik A, Yoshie O. Chemokines: a new classification system and their role in immunity. Immunity 2000;12:121–7.
[2] Horuk R. Chemokine receptors. Cytokine Growth Factor Rev 2001;12:313–35.
[3] Feng Y, Broder CC, Kennedy PE, Berger EA. HIV-1 entry cofactor: functional cDNA cloning of a seven-transmembrane, G protein-coupled receptor. Science 1996;272:872–7.
[4] Müller A, Homey B, Soto H, Ge N, Catron D, Buchanan ME, et al. Involvement of chemokine receptors in breast cancer metastasis. Nature 2001;410:50–6.
[5] Taichman RS, Cooper C, Keller ET, Pienta KJ, Taichman NS, McCauley RS. Use of the stromal cell-derived factor-1/CXCR4 pathway in prostate cancer metastasis to bone. Cances Res 2002;62: 1832–7.
[6] Schrader AJ, Lechner O, Templin M, Dittmar KEJ, Machtens S, Mengel M, et al. CXCR4/CXCL12 expression and signaling in kidney cancer. Br J Cancer 2002;86:1250–6.
[7] Phillips RJ, Burdick MD, Lutz M, Belperio JA, Keane MP, Strieter RM. The stromal derived factor-1/CXCL12-CXC chemokine receptor 4 biological axis in non-small cell lung cancer metastases. Am J Respir Crit Care Med 2003;167:1676–86.
[8] Uchida D, Begum NM, Almofti A, Nakashiro K, Kawamata H, Tateishi Y, et al. Possible role of stromal-cell-derived factor-1/CXCR4 signaling on lymph node metastasis of oral squamous cell carcinoma. Exp Cell Res 2003;290:289–302.
[9] Masuda M, Nakashima H, Ueda T, Naba H, Ikoma R, Otaka A, et al. A novel anti-HIV synthetic peptide, T-22 ([Tyr^{5,12}Lys^{7}]-polyphemusin II). Biochem Biophys Res Commun 1992;189:845–50.
[10] Murakami T, Nakajima T, Koyanagi Y, Tachibana K, Fujii N, Tamamura H, et al. A small molecule CXCR4 inhibitor that blocks T cell line-tropic HIV-1 infection. J Exp Med 1997;186: 1389–93.
[11] Tamamura H, Arakaki R, Funakoshi H, Imai M, Otaka A, Ibuka T, et al. Effective lowly cytotoxic analogs of an HIV-cell fusion inhibitor, T22 ([Tyr^{5,12},Lys^{7}]-polyphemusin II). Bioorg Med Chem 1998;6:231–8.
[12] Tamamura H, Xu Y, Hattori T, Zhang X, Arakaki R, Kanbara K, et al. A low-molecular- weight inhibitor against the chemokine receptor

CXCR4: a strong anti-HIV peptide T140. Biochem Biophys Res Commun 1998;253:877–82.

[13] Tamamura H, Omagari A, Oishi S, Kanamoto T, Yamamoto N, Peiper SC, et al. Pharmacophore identification of a specific CXCR4 inhibitor, T140, leads to development of effective anti-HIV agents with very high selectivity indexes. Bioorg Med Chem Lett 2000;10:2633–7.

[14] Tamamura H, Sugioka M, Odagaki Y, Omagari A, Kan Y, Oishi S, et al. Conformational study of a highly specific CXCR4 inhibitor, T140, disclosing the close proximity of its intrinsic pharmacophores associated with strong anti-HIV activity. Bioorg Med Chem Lett 2001;11:359–62.

[15] Tamamura H, Sugioka M, Odagaki Y, Omagari A, Kan Y, Oishi S, et al. Corrigendum to "conformational study of a highly specific CXCR4 inhibitor, T140, disclosing the close proximity of its intrinsic pharmacophores associated with strong anti-HIV activity" [Bioorg. Med. Chem. Lett. 11 (2001) 359]. Bioorg Med Chem Lett 2001;11:2409.

[16] Tamamura H, Omagari A, Hiramatsu K, Gotoh K, Kanamoto T, Xu Y, et al. Development of specific CXCR4 inhibitors possessing high selectivity indexes as well as complete stability in serum based on an anti-HIV peptide T140. Bioorg Med Chem Lett 2001;11:1897–902.

[17] Tamamura H, Hiramatsu K, Kusano S, Terakubo S, Yamamoto N, Trent JO, et al. Synthesis of potent CXCR4 inhibitors possessing low cytotoxicity and improved biostability based on T140 derivatives. Org Biomol Chem 2003;1:3656–62.

[18] Arano Y, Uezono T, Akizawa H, Ono M, Wakisaka K, Nakayama M, et al. Reassessment of diethylenetriaminepentaacetic acid (DTPA) as a chelating agent for indium-111 labeling of polypeptides using a newly synthesized monoreactive DTPA derivative. J Med Chem 1996;39: 3451–60.

[19] Arano Y, Akizawa H, Uezono T, Akaji K, Ono M, Funakoshi S, et al. Conventional and high-yield synthesis of DTPA-conjugated peptide: application of a monoreactive DTPA to DTPA-D-Phe^1-octreotide synthesis. Bioconjug Chem 1997;8:442–6.

[20] Hesselgesser J, Liang M, Hoxie J, Greenberg M, Brass LF, Orsini MJ, et al. Identification and characterization of CXCR4 chemokine receptor in human T cell lines: ligand binding, biological activity, and HIV-1 infectivity. J Immunol 1998;160:877–83.

[21] Tamamura H, Omagari A, Hiramatsu K, Oishi S, Habashita H, Kanamoto T, et al. Certification of the critical importance of L-3-(2-naphthyl)alanine at position 3 of specific CXCR4 inhibitor, T140, leads to an exploratory performance of its downsizing study. Bioorg Med Chem 2002;10:1417–26.

[22] Grynkiewicz G, Poenie M, Tsien RY. A new generation of Ca^{2+} indicators with greatly improved fluorescence properties. J Biol Chem 1985;260:3440–50.

[23] Koshiba T, Hosotani R, Miyamoto Y, Ida J, Tsuji S, Nakajima S, et al. Expression of stromal cell-derived factor 1 and CXCR4 ligand receptor system in pancreatic cancer: a possible role for tumor progression. Clin Cancer Res 2000;6:3530–5.

[24] Mori T, Doi R, Koizumi M, Toyoda E, Ito D, Kami K, et al. CXCR4 antagonist inhibits stromal cell-derived factor 1-induced migration and invasion of human pancreatic cancer. Mol Cancer Ther 2004;3: 29–37.

[25] Nagasawa T, Nakajima T, Tachibana K, Iizasa H, Bleul CC, Yoshie O, et al. Molecular cloning and characterization of a murine pre-B-cell growth-stimulating factor/stromal cell-derived factor 1 receptor, a murine homolog of the human immunodeficiency virus 1 entry coreceptor fusin. Proc Natl Acad Sci U S A 1996;93:14726–9.

[26] Moepps B, Frodl R, Rodewald HR, Bsggiolini M, Gierschik P. Two murine homologues of the human chemokine receptor CXCR4 mediating stromal cell-derived factor 1α activation of G_{i2} are differentially expressed in vivo. Eur J Immunol 1997;27: 2102–12.

[27] de Jong M, Rolleman EJ, Bernard BF, Visser TJ, Bakker WH, Breeman WAP, et al. Inhibition of renal uptake of indium-111-DTPA-octreotide in vivo. J Nucl Med 1996;37:1388–92.

[28] Akizawa H, Arano Y, Mifune M, Iwado A, Saito Y, Mukai T, et al. Effect of molecular charges on renal uptake of ^{111}In-DTPA-conjugated peptides. Nucl Med Biol 2001;28:761–8.

[29] Akizawa H, Takimoto H, Saito M, Iwado A, Mifune M, Saito Y, et al. Effect of carboxylation of N-terminal phenylalanine of ^{111}In-DTPA (diethylenetriaminepentaacetic acid)-octreotide on accumulation of radioactivity in kidney. Biol Pharm Bull 2004;27:271–2.

[30] Bagutti C, Stolz B, Albert R, Bruns C, Pless J, Eberle AN. [^{111}In]-DTPA-labeled analogues of α-melanocyte-stimulating hormone for melanoma targeting: receptor binding in vitro and in vivo. Int J Cancer 1994;58:749–55.

[31] de Visser M, Janssen PJJM, Srinvasan A, Reubi JC, Waser B, Erion JL, et al. Stabilised ^{111}In-labelled DTPA- and DOTA-conjugated neurotensin analogues for imaging and therapy of exocrine pancreatic cancer. Eur J Nucl Med Mol Imaging 2003;30:1134–9.

[32] Schimanski CC, Schwald S, Simiantonaki N, Jayasinghe C, Gonner V, Wilsberg V, et al. Effect of chemokine receptors CXCR4 and CCR7 on the metastatic behavior of human colorectal cancer. Clin Cancer Res 2005;11:1743–50.

[33] Kim J, Takeuchi H, Lam ST, Turner RR, Wang HJ, Kuo C, et al. Chemokine receptor CXCR4 expression in colorectal cancer patients increases the risk for recurrence and for poor survival. J Clin Oncol 2005;23:2744–53.

[34] Scala S, Ottaiano A, Ascierto PA, Cavalli M, Simeone E, Giuliano P, et al. Expression of CXCR4 predicts poor prognosis in patients with malignant melanoma. Clin Cancer Res 2005;11:1835–41.

[35] Laverdiere C, Hoang BH, Yang R, Sowers R, Qin J, Meyers PA, et al. Messenger RNA expression levels of CXCR4 correlate with metastatic behavior and outcome in patients with osteosarcoma. Clin Cancer Res 2005;11:2561–7.

[36] Tamamura H, Hori A, Kanzaki N, Hiramatsu K, Mizumoto M, Nakashima H, et al. T140 analogs as CXCR4 antagonists identified as anti-metastatic agents in the treatment of breast cancer. FEBS Lett 2003;550:79–83.

[37] Liang Z, Wu T, Lou H, Yu X, Taichman RS, Lau SK, et al. Inhibition of breast cancer metastasis by selective synthetic polypeptide against CXCR4. Cancer Res 2004;64:4302–8.

[38] Takenaga M, Tamamura H, Hiramatsu K, Nakamura N, Yamaguchi Y, Kitagawa A, et al. A single treatment with micro-capsules containing a CXCR4 antagonist suppresses pulmonary metastasis of murine melanoma. Biochem Biophys Res Commun 2004;320:226–32.

[39] Smith MC, Luker KE, Garbow JR, Prior JL, Jackson E, Piwnica-Worms D, et al. CXCR4 regulates growth of both primary and metastatic breast cancer. Cancer Res 2004;64:8604–12.

HETEROCYCLES, Vol. 70, 2006, pp. 501 - 508. © The Japan Institute of Heterocyclic Chemistry
Received, 29th September, 2006, Accepted, 15th November, 2006, Published online, 17th November, 2006. COM-06-S(W)51

PHOTOCHEMICAL SYNTHESIS OF POLYCYCLIC PYRIMIDINES THROUGH THE ACID CATALYZED CYCLOADDITION OF 6-CHLORO-1-METHYLURACIL TO METHYL SUBSTITUTED BENZENES

Kazue Ohkura,*[a] Takeshi Yamaguchi,[a] Ken-ichi Nishijima,[a] Yuji Kuge,[b] and Koh-ichi Seki[b]

[a] Faculty of Pharmaceutical Sciences, Health Sciences University of Hokkaido, Ishikari-Tobetsu, Hokkaido 061-0293, Japan
[b] Graduate School of Medicine, Hokkaido University, Kita-15, Nishi-7, Kita-ku, Sapporo 060-0815, Japan
E-mail: ohkura@hoku-iryo-u.ac.jp

Abstract – UV-irradiation of 6-chloro-1-methyluracil with benzene in the presence of TFA resulted in 1,2-cycloaddition and susequent elimination of HCl gave a cyclooctapyrimidine-2,4-dione. Similar acid catalyzed photoreaction with substituted benzenes bearing two or three methyl groups afforded the corresponding cyclooctapyrimidines and two novel pentacyclic compounds, 9,11-diazapentacyclo[6.4.0.0^{1,3}.0^{2,5}.0^{4,8}]dodecanes and 9.11-diazapentacyclo[6.4.0.0^{1,3}.0^{2,6}.0^{4,8}]dodcanes, in fair yields.

Recently, photoreaction of nucleic bases has been received much attention from both organic chemistry and biological perspectives.[1] During the course of our continuing studies on the photochemical modification of the pyrimidine ring, we have previously reported that the acid catalyzed photoreaction of 6-chloro-1,3-dimethyluracil (6-ClDMU) with benzene derivatives proceeds by way of 1,2-cycloaddition to give cyclooctapyrimidines.[2] Certain cyclooctapyrimidines were further converted into various novel valence isomers,[3-5] by way of a variety of electrocyclic pathways depending on the reaction conditions and substituents on the cycloadducts. These reactions however, have been carried out with both *N*1 and *N*3 methyl capped uracils. Taking the biological importance of the *N*3-H moiety of the pyrimidine ring into consideration, the presence of a non-protected *N*3-H function of the pyrimidine ring

This paper is dedicated to Professor Steven M. Weinreb on the occasion of his 65th birthday.

may represent a significant pharmacophore for the development of useful chemotherapeutics. We intended to extend this photoreaction to 6-chloro-1-methyluracil (**1**) bearing an *N*3-H function. In the present paper, we describe that the photoreaction of **1** with benzene and its methyl derivatives in the presence of TFA successfully effected cycloaddition to give NH free polycyclic pyrimidines.

UV-irradiation of a solution of 6-chloro-1-methyluracil (**1**) in benzene (**2a**) with a 500 W high-pressure mercury lamp in a degassed Pyrex tube (λ>300 nm) for 16 h afforded 1-methyl-6-phenyluracil (**3a**) in low yield (3%), together with large amount of unreacted **1**. In contrast, the addition of TFA to the solution gave rise to the formation of 1-methylcyclooctapyrimidine-2,4-dione (**4a**) in appreciable yield (70%, based on 73% **1** consumed), while the substitution reaction was significantly attenuated (3%) (Scheme 1).

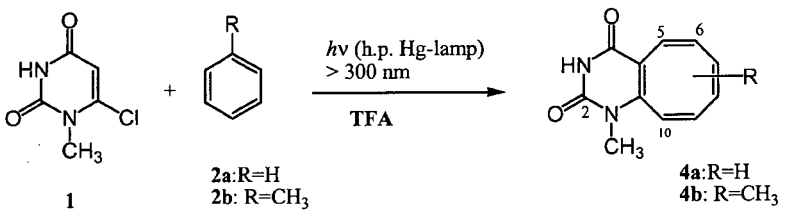

Scheme 1

The structural assignment of **4a** was made on the basis of detailed MS and the NMR spectroscopic studies. The coupling constants for the vinyl protons of **4a**, $J_{5,6}$, $J_{7,8}$, $J_{9,10}$ = 11.5 Hz, and $J_{6,7}$, $J_{8,9}$, = 3.5-4 Hz, revealed the configurations to be all *cis*.

The photoreaction with toluene (**2b**) under the above conditions afforded five isomeric 1,*n*-dimethyl-cyclooctapyrimidines (*n*=6,7,8,9,10) in fair yield (**4b**$_6$:23%, **4b**$_7$: 16%, **4b**$_8$: 25%, **4b**$_9$: 7%, **4b**$_{10}$: 18%) (Scheme1). The structural assignments, including the stereochemistry of **4b** were made on the basis of the similarity to **4a** in their ^{1}H-NMR spectroscopic data. Methyl substituted sites on the cycloocta-tetraene moiety were determined by NOE experiments.

Thus, analogous to the case of the reaction with 6-ClDMU and **2a,b**, UV excitation of **1** undergoes 1,2-cycloaddition with **2a,b** to produce cyclooctapyrimidines *via* the concomitant elimination of hydrogen chloride which is then followed by an electrocyclic ring opening reaction.

We then investigated the photoreaction with *p*-xylene (**2c**) under the same conditions. HPLC separation of the reaction mixture afforded three types of cycloadducts as single regioisomers namely, 1, 7,10-trimethylcyclooctapyrimidine-2,4-dione (**4c**) in 31% yield along with two novel pentacyclic compounds, 6-methylene-3,9-dimethyl-9,11-diazapentacyclo[6.4.0.0^{1,3}.0^{2,5}.0^{4,8}]dodecane-10,12-dione (**5c**) and 5-methylene-2,9-dimethyl-9,11-diazapentacyclo[6.4.0.0^{1,3}.0^{2,6}.0^{4,8}]dodecane-10,12-dione (**6c**)

in 15% and 13 % yield respectively. Conversely, the reaction with toluene gave the cyclooctapyrimidines with poor regioselectivity (Scheme 2).

The structures of **5c** and **6c** were determined by comparison with the NMR data for *N*3-methyl penta-

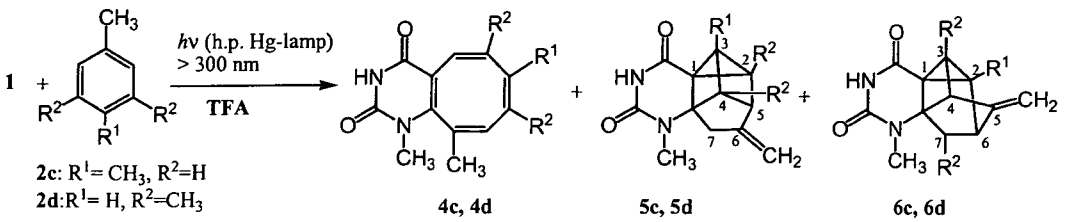

Scheme 2

cyclic derivatives which had given X-ray crystallographic data in detail.[6] The ^{1}H and ^{13}C-nmr spectra including ^{13}C-^{1}H COSY showed signals due to two methyl groups, two methylene groups, three methine groups and six quaternary carbon atoms. HMBC spectrum and NOE experiments provided the information to enable us to construct pentacyclic compounds consisting of 3, 4, 4, and 5-membered rings for **5c** and 3, 4, 5, and 5-membered rings for **6c**.

Similarly the photoreaction with mesitylene (**2d**) afforded 1,6,8,10-tetramethyl-cyclooctapyrimidine-2,4-dione (**4d**) (21%) and the two pentacyclic compounds, 6-methylene-2,4,9-trimethyl-9,11-diazapentacyclo[6.4.0.0^{1,3}.0^{2,5}.0^{4,8}]dodecane-10,12-dione (**5d**) (18%) and 5-methylene-3,7,9-trimethyl-9,11-diazapentacyclo[6.4.0.0^{1,3}.0^{2,6}.0^{4,8}] dodecane-10,12-dione (**6d**) (8%) (Scheme 2).

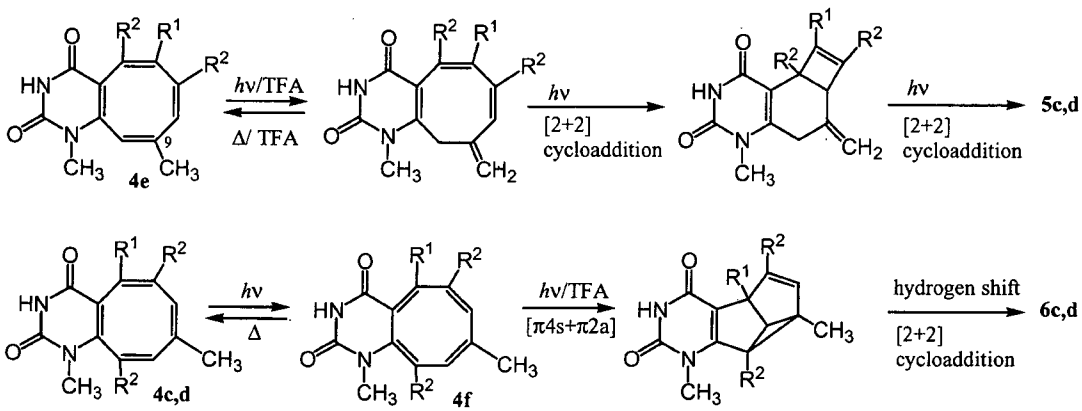

Scheme 3

The reaction pathway for the formation of the pentacyclic compound is inferred on the basis of the established pathway[7] for the formation of *N*3-methyl derivative respectively as depicted in Scheme 3. It

is suggested that compound **5** could be derived from 9-methylcyclooctapyrimidine (**4e**) *via* a multi-step transformation starting with a [1,3] sigmatropic rearrangement of 9-methyl group followed by subsequent double [2 + 2] cycloaddition processes. The formation of compound **6** can be explained by the rearrangement of cyclooctapyrimidine tautomer (**4f**) involving a [π4s +π2a] process.

These results provide the first example of the formation of various cycloadducts between *N*3-H chlorouracil and benzenes. Interestingly in this reaction methyl substituents on the benzene ring are effective auxiliaries in achieving subsequent electrocyclic rearrangement of photoadducts including forming highly strained pentacyclic cage compounds.

It is noteworthy that reactions involving *N*3 free 6-chlororouracil in place of dimethyluracil derivatives, would provide synthons for the synthesis of singular polycyclic systems including a *N*3 non-substituted pyrimidine ring.

EXPERMENTAL

NMR spectra were measured with a JEOL JNM-EA500 (500 MHz) spectrometer, and ^{1}H-NMR chemical shifts are given on the δ(ppm) scale based on those of the signals of solvents. MS spectra and high-resolution MS (HRMS) spectra were recorded with JEOL JMS-FABmate (EI). Reverse-phase liquid chromatography (RP-HPLC) was carried out on a Shim-pac PREP-ODS (25 cm x 20 mm *i.d.*) (Shimadzu) with aqueous methanol, using a Shimadzu LC-6A apparatus with monitoring at 254 nm. Silica gel LC (Si-HPLC) was conducted on a Shim-pac PREP-Sil (H) (25 cm x 20 mm *i.d.*) (silica gel), using the same apparatus. UV-Irradiation was carried out externally with a 500 W high-pressure mercury (h. p. Hg) lamp (Eiko-sha, Osaka) in a degassed Pyrex tube (> 300 nm) on a merry-go-round apparatus.

Photoreaction of 1 with 2 in the presence of TFA----- A solution of **1** (56 mg, 0.35 mmol) and TFA (10 equiv. mol: 260 μl) in benzenes (**2a-d**) (100 mL) was put portion-wise (10 mL each) into ten degassed Pyrex tubes and irradiated externally at room temperature for 16 h.

Typical procedure for the isolation of the cycloadduct----- After the photoreaction according to the general procedure, the reaction mixtures in several Pyrex tubes were put together, and evaporated *in vacuo*. The residual oil was passed through a short column of silica gel with AcOEt. The eluate was submitted to HPLC with following solvent systems; 30% MeOH-H_2O on RP-HPLC for **4a**, 15% AcOEt-hexane on Si-HPLC for **4b**, **4d**, **5d**, and **6d**, and 25% AcOEt- hexane on Si-HPLC for **4c**, **5c**, and **6c**.

1-Methylcyclooctapyrimidine-2,4-dione(4a): Yellow crystals, mp 243-246 °C (*i*-PrOH). ^{1}H–NMR

(C_6D_6) δ; 2.45 (3H, s, N^1-CH_3), 4.92 (1H, d, *J*=11.5 Hz, H-10), 5.41 (1H, dd, *J*=11.5, 3.5 Hz, H-9), 5.47 (1H, dd, *J*=11.5, 3.5 Hz, H-8), 5.58 (1H, dd, *J*=11.5, 4.0 Hz, H-7), 5.66 (1H, dd, *J*=11.5, 4.0 Hz, H-6), 6.24 (1H, d, *J*=11.5 Hz, H-5), 9.13 (1H, brs, N^3-H). NOE; H-10 with N^1-CH_3 , H-9; H-5 with H-6; N^1-CH_3 with H-10. ^{13}C-NMR (C_6D_6); 30.47 (N^1-CH_3), 110.83 (4a), 125.74 (10), 127.55 (5), 129.33 (9), 130.79 (6), 133.05 (7), 135.39 (8), 149.16 (10a), 150.68 (2), 161.00 (4). MS *m/z* (%):202 (M^+, 100), 159 (55), 131 (42), 116 (32). *Anal.* Calcd for $C_{11}H_{10}N_2O_2$: C, 65.34; H, 4.98; N, 13.85. Found: C, 65.27; H, 4.99; N, 13.77.

1,6-Dimethylcyclooctapyrimidine-2,4-dione(4b$_6$): Yellow crystals, mp 220-223 °C (acetone). ^{1}H-NMR($CDCl_3$) δ; 1.86 (3H, s, C^6-CH_3), 3.28 (3H, s, N^1-CH_3), 5.89 (1H, s, H-5), 5.94 (1H, dd, *J*=11.5, 3.5 Hz, H-8), 6.01 (1H, d, *J*=11.5 Hz, H-7), 6.01 (1H, d, *J*=11.5 Hz, H-10), 6.31 (1H, dd, *J*=11.5, 3.5 Hz, H-9), 8.38 (1H,brs,N^3-H). NOE; H-10 with N^1-CH_3, H-9; H-9 with H-10, H-8; H-8 with H-9, H-7; H-7 with H-8, C^6-CH_3 ; C^6-CH_3 with H-7, H-5. ^{13}C-NMR($CDCl_3$) δ; 23.45 (C^6-CH_3), 31.88 (N^1-CH_3), 112.50 (4a), 121.63 (5), 125.56 (10), 127.86 (8), 136.44 (7), 136.93 (9), 140.93 (6), 149.79 (10a), 151.03 (2), 161.79 (4). MS *m/z* (%):216 (M^+, 100), 201 (11), 173 (38), 158 (18), 145 (39), 115 (14), 104 (18). HRMS; Calcd for $C_{12}H_{12}N_2O_2$: 216.0899. Found: 216.0902.

1,7-Dimethylcyclooctapyrimidine-2,4-dione(4b$_7$): Yellow crystals, mp 227-230 °C (*i*-PrOH). ^{1}H-NMR($CDCl_3$) δ; 1.78 (3H, s, C^7-CH_3), 3.28 (3H, s, N^1-CH_3), 5.74 (1H, m, H-8), 5.92 (1H, d, *J*=11.5 Hz, H-10), 5.97 (1H, d, *J*=11.5 Hz, H-6), 6.09 (1H, d, *J*=11.5 Hz, H-5), 6.27 (1H, dd, *J*=11.5, 3.5 Hz, H-9), 8.64 (1H, brs, N^3-H9). NOE; H-10 with N^1-CH_3, H-9; H-9 with H-10, H-8; H-8 with H-9, C^7-CH_3; C^7-CH_3 with H-8, H-6. ^{13}C-NMR ($CDCl_3$); 23.38 (C^7-CH_3), 31.80 (N^1-CH_3), 111.51 (4a), 124.47 (10), 124.90 (8), 124.93 (5), 135.49 (6), 137.91 (9), 141.83 (7), 150.63 (10a), 151.05 (2), 161.51 (4). MS *m/z* (%):216 (M^+, 100), 201 (15), 173 (27), 158 (18), 145 (33), 130 (22), 115 (9), 104 (22). *Anal.* Calcd for $C_{12}H_{12}N_2O_2$ C, 66.65; H, 5.59; N, 12.96. Found: C, 65.90; H, 5.52; N, 12.51.

1,8-Dimethylcyclooctapyrimidine-2,4-dione(4b$_8$): Yellow crystals, mp 207-210 °C (*i*-PrOH). ^{1}H-NMR($CDCl_3$) δ; 1.82 (3H, s, C^8-CH_3), 3.29 (3H, s, N^1-CH_3), 5.77 (1H, m, H-7), 5.93 (1H, d, *J*=11.5 Hz, H-10), 6.00 (1H, dd, *J*=11.5, 3.5 Hz, H-6), 6.10 (1H, d, *J*=11.5 Hz, H-5), 6.23 (1H, d, *J*=11.5 Hz, H-9). NOE; H-10 with N^1-CH_3 , H-9; H-9 with H-10, C^8-CH_3; C^8-CH_3 with H-9, H-7; H-7 with C^8-CH_3, H-6; H-6 with H-7, H-5; N^1-CH_3 with H-10. ^{13}C-NMR ($CDCl_3$) δ; 22.48 (C^8-CH_3), 31.73 (N^1-CH_3), 111.60 (4a), 123.73 (10), 125.72 (5), 127.85 (7), 133.03 (6), 138.37 (8), 140.02 (9), 150.17 (10a), 151.26 (2), 161.77 (4). MS *m/z* (%):216 (M^+, 100), 201 (11), 176 (23), 173 (26), 158 (14), 145 (37), 144 (34), 130 (32), 115 (12), 104 (30). HRMS; Calcd for $C_{12}H_{12}N_2O_2$: 216.0899. Found: 216.0895.

1,9-Dimethylcyclooctapyrimidine-2,4-dione(4b$_9$): Yellow crystals, mp 245-247 °C (acetone). ^{1}H-